Tunable thermal conduction force without macroscopic temperature gradients

Haohan Tan,[1] Yuguang Qiu,[1] Liujun Xu,[2,*] and Jiping Huang[1,†]

[1]*Department of Physics, State Key Laboratory of Surface Physics, and Key Laboratory of Micro and Nano Photonic Structures (MOE), Fudan University, Shanghai 200438, China*

[2]*Graduate School of China Academy of Engineering Physics, Beijing 100193, China*

(Received 17 February 2023; accepted 17 August 2023; published 7 September 2023)

Ubiquitous thermal conduction makes its force effect particularly important in diverse fields, such as electronic engineering and biochemistry. However, regulating thermal conduction force is still challenging due to two stringent restrictions. First, a temperature gradient is essential for inducing the force effect. Second, the force direction is fixed to the temperature gradient in a specific material. Here, we demonstrate that thermal conduction force can exist unexpectedly at a zero average temperature gradient in dielectric crystals. The wavelike feature of thermal conduction is considered, i.e., the second sound mode. Based on the momentum conservation law for phonon gases, we analyze thermal conduction force with the plane, zeroth-order Bessel, and first-order Bessel second sounds. Remarkably, the force direction is highly tunable to be along or against the second sound direction. These results provide valuable insights into thermal conduction force in those environments with temperature fluctuations, and they open up possibilities for practical applications in manipulating the local thermal conductivity of crystals.

DOI: 10.1103/PhysRevE.108.034105

I. INTRODUCTION

Thermal conduction, a primary mode of heat transfer, is essential for life and industry [1–3]. At a microscopic level, it is described by phonon motion [4,5]. As phonons carry energy and momentum, they can interact with an object in the thermal conduction path and produce a force on the object through momentum exchange. Based on the hypothesis that heat flux interacts with momentum flux [6,7], thermal conduction force was predicted in the liquid-liquid or liquid-solid phase with a constant temperature gradient, and its effect was experimentally detected [8]. However, existing research on thermal conduction force has mainly focused on liquids, ignoring the ubiquitous solid-solid phase. Moreover, a constant temperature gradient is necessary to induce the force effect, similar to the condition for observing thermophoresis [9,10]. The force direction is also fixed to the temperature gradient in a specific material, which severely limits the flexibility of thermal conduction force regulation. Therefore, studying tunable thermal conduction force in solid-solid phases without macroscopic temperature gradients remains a challenging task.

The second sound mode has been shown to exhibit wavelike behavior in dielectric crystals [11,12], resulting in a periodic temperature field in space and time, and thus a zero macroscopic temperature gradient. This is distinct from the diffusive nature of thermal conduction [13,14]. However, investigating the force effect of second sounds [herein referred to as the second sound radiation force (SSRF)] is still challenging due to several tricky problems. On the one hand, the nonlinearity of second sounds leads to the failure of the Fourier law [15–17]. On the other hand, when second sounds propagate in dielectric crystals, the phonon model describing thermal conduction is nonequilibrium, resulting in a highly complicated case. Despite various experimental evidence of second sounds [18–24], exploring the interaction between second sounds and impurities remains elusive.

Here, we propose the fundamental theory of the SSRF based on the momentum conservation law in phonon systems. Considering a low temperature and only one branch of lattice waves, we first investigate the SSRF of the plane second sound (PSS) and zeroth-order Bessel second sound (ZBSS) on a fixed spherical particle with the scattering theory; see Figs. 1(a) and 1(b). Despite the pattern difference of second sounds, the SSRF direction is always along the propagating path of second sounds, demonstrating a pushing effect on the particle. We further study the SSRF of the first-order Bessel second sound (FBSS), whose direction can be unexpectedly opposite to the FBSS propagating direction, exhibiting a dragging effect on the particle. The underlying mechanism is that the scattering properties of different incident second sounds are distinct, thus showing distinct characteristics. These results help flexibly change the local phonon spectrum and realize local thermal conductivity manipulation; see Fig. 1(c).

II. GENERAL THEORY FOR CALCULATING THERMAL CONDUCTION FORCE

Without loss of generality, we start with a simple model to investigate the SSRF and consider a crystal where the second sound propagation is lossless. The temperature is about 10 K, a typical value ensuring that phonon transport is in the hydrodynamic regime [12]. The resistive relaxation time τ_R is nearly

*ljxu@gscaep.ac.cn
†jphuang@fudan.edu.cn

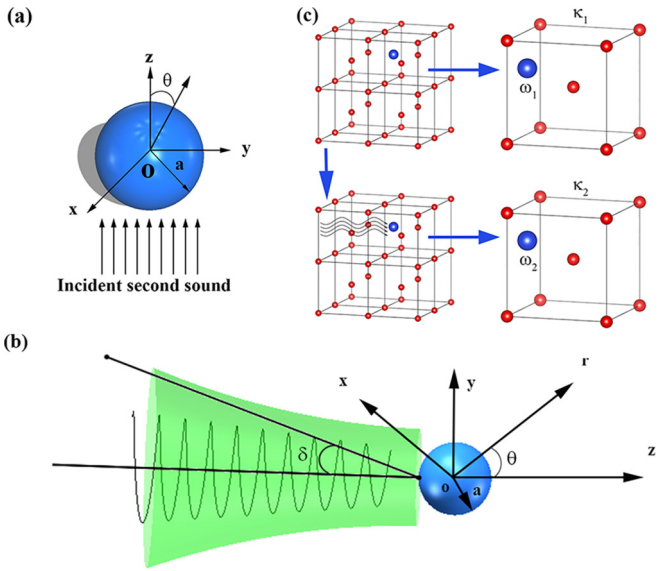

FIG. 1. Schematic of thermal conduction force. (a) An adiabatic spherical particle with a radius a in the presence of an incident second sound propagating along the z axis is depicted. The particle center is the origin of the Cartesian coordinate system (x, y, z), and θ denotes the polar angle. (b) A particle in the presence of the Bessel second sound is shown, with δ representing the cone angle. (c) The local thermal conductivity of dielectric crystals can be tuned by manipulating the interaction between the impurity particle (the blue sphere) and the second sound (the black wave line). ω_1 and ω_2 are the vibrating angular frequencies of the impurity particle before and after interacting with the second sound, and κ_1 and κ_2 are the corresponding local thermal conductivities of the crystal. The region containing the impurity particle is zoomed in for clarity.

infinite, i.e., $\tau_R \to \infty$, indicating that the resistive process can be ignored. Consequently, the collisions between phonons keep the total momentum conservation. The normal relaxation time τ_N is short, making the collisions between phonons sufficiently frequent, and the phonon system can reach the local equilibrium state. In natural crystals, the resistive process inevitably exists, resulting in the second sound attenuation during propagation. However, when $\tau_N \ll \tau_R$, the resistive process can be neglected [25]. Therefore, adopting the no-attenuation model is reasonable. Under this circumstance, the local equilibrium distribution function of the phonon system is

$$f(\boldsymbol{k}, \boldsymbol{r}, t) = \frac{1}{e^{\beta(\boldsymbol{r},t)[\hbar\omega_k - \hbar\boldsymbol{k}\cdot\boldsymbol{u}(\boldsymbol{r},t)]} - 1}, \tag{1}$$

where $\hbar$, ω_k, $\boldsymbol{k}$, and $\boldsymbol{u}(\boldsymbol{r}, t)$ are the reduced Planck constant, phonon angular frequency, phonon wave vector, and phonon drifting velocity, respectively. $\beta(\boldsymbol{r}, t) = 1/[k_B T(\boldsymbol{r}, t)]$, where k_B is the Boltzmann constant, and $T(\boldsymbol{r}, t)$ is the local temperature of the crystal. $\boldsymbol{r}$ is the position vector, and t represents time. Since the temperature and drifting velocity vary spatiotemporally, the phonon system is in a nonequilibrium state. This state is distinct from the equilibrium state, whose distribution function is given by

$$f_0(\boldsymbol{k}) = \frac{1}{e^{\beta_0\hbar\omega_k} - 1}, \tag{2}$$

where $\beta_0 = 1/(k_B T_0)$ is a constant and T_0 is the background temperature. In fact, when calculating the thermal conduction force, the size of the impurity plays a significant role and should be taken into consideration. As a starting point for our calculations, we make use of the local equilibrium assumption for the phonon system. It is important to note that as the size of the impurity varies, the relaxation time τ_R also changes, which can be referred to as the size effect. However, in this paper, regardless of how τ_R changes, our focus remains on the second sound region, where $\tau_N \ll \tau_R$. Consequently, we can still assume that the phonon system is in a state of local equilibrium. We use the Debye model to describe the phonon spectrum, i.e., $\omega_k = c|\boldsymbol{k}|$, where c is a constant representing the modulus of phonon group velocity and implicitly related to the lattice potential field. The velocities of the longitudinal and transverse waves are equal. According to the Debye model, we should consider the contribution of one longitudinal wave and two transverse waves. However, considering only one branch of lattice waves does not affect the results qualitatively [26]; thus, we only consider the contribution of the longitudinal wave. Substituting the first-order Taylor expansion for f into the energy and momentum conservation laws for the phonon system (see Appendix A), we derive

$$\frac{\partial}{\partial t}E(r, t) + \frac{\partial}{\partial r_i}Q_i(r, t) = 0, \tag{3}$$

$$\frac{\partial}{\partial t}P_i(r, t) + \frac{\partial}{\partial r_j}\Pi_{ij}(r, t) = 0, \tag{4}$$

where E represents the energy density, while Q_i, P_i, and Π_{ij} denote the components of energy flux vector, momentum density vector, and momentum flux tensor of the phonon system, respectively. The subscripts i or j take x, y, and z, indicating that the corresponding components, e.g., r_x, r_y, and r_z denote the coordinate components of $\boldsymbol{r}$. For repeated subscripts, the Einstein summation convention is used. We obtain the dynamic equations for β and $\boldsymbol{u}$,

$$\left(\frac{\partial^2}{\partial t^2} - \frac{c^2}{3}\nabla^2\right)\beta(r, t) = 0, \tag{5}$$

$$\left(\frac{\partial^2}{\partial t^2} - \frac{c^2}{3}\nabla^2\right)\boldsymbol{u}_i(r, t) = 0, \tag{6}$$

where ∇^2 is the Laplace operator in three dimensions. Equation (5) shows that the temperature field propagates as a wave [26–29], i.e., the second sound mode.

We consider a fixed spherical impurity with a radius a in a crystal. The particle boundary is adiabatic, forbidding the propagation of second sound. The incident second sound interacts with the impurity and is scattered during propagation. The time-averaged force containing the influence of incident and scattered second sounds on the particle is the SSRF. Since the second sound is a continuous sinusoidal wave, we define the SSRF based on the momentum conservation law,

$$F = -\iint \langle \Pi' \rangle dS, \tag{7}$$

where $\Pi'_{ij} = \sum_k \hbar k_i v_{k_j}(f - f_0)$ is the momentum flux of the second sound, and $v_{k_j} = \partial\omega_k/\partial k_j$ is the phonon group velocity component. No second sound appears when the phonon

system is in equilibrium. We should ignore the contribution of f_0 to explore the SSRF, which is illustrated by $f - f_0$ in the definition. The integration is over the particle surface S, with the particle center being the origin of the Cartesian coordinate system (x, y, z); see Fig. 1(a). The propagating direction of the second sound is along the z axis. We only consider the SSRF along the propagating direction, and we obtain

$$F = -\iint \sum_k \hbar k_z v_{k_z} (f - f_0) dS. \tag{8}$$

The SSRF does not exist unless we perform a Taylor expansion of f to at least the second order (see Appendix B). The general expression of the SSRF is

$$F = -\frac{1}{2} \times \iint \left(\frac{2\pi^2}{9\beta_0^4(\hbar c)^3} \left\langle \left(\frac{T_1^{'}}{T_0} \right)^2 \right\rangle + \frac{\pi^2}{15\beta_0^4 \hbar^3 c^5} \left\langle |u|^2 \right\rangle \right) dS, \tag{9}$$

where $T_1^{'}$ is the temperature deviation from the background temperature. Then we should calculate the average value of $T_1^{'2}$ and $|u|^2$. In this paper, we employ the multipole expansion-based method for the direct calculation of thermal conduction force. In the field of acoustics, there are two distinct approaches for computing the acoustic radiation force and torque: the angular spectrum-based method and the multipole expansion-based method. These methods differ in how they decompose the incident wave. The former method decomposes the incident wave into a series of plane waves [30,31], while the latter method decomposes it into a sum of spherical waves [32–35]. Each method offers its own advantages. The advantage of the angular spectrum-based method lies in its direct calculation of the acoustic radiation force and torque. On the other hand, the multipole expansion-based method is advantageous due to its ease of setup. However, Gong *et al.* have demonstrated the equivalence between these two methods [36]. The second sound wavelength l, the normal relaxation time τ_N, and the second sound speed c_s satisfy $l = \tau_N c_s$, so the second sound wavelength is about a micrometer [37], much longer than the lattice constant (about 20 Å) in natural crystals. Thus, we ignore the lattice effect.

III. PUSHING AND PULLING EFFECTS WITH DIFFERENT INCIDENT SECOND SOUNDS

We further explore the SSRF with three kinds of second sounds. First, we consider the SSRF with the plane second sound (PSS). Though the PSS solution is the simplest one to Eq. (5), many typical characteristics of the SSRF can be revealed. Temperature pulses or optical methods could excite an approximate PSS. The PSS propagating along the z axis can be described by $T_{inc} = T_0 + T_1 e^{i(qz-\omega t)}$, where T_1, q, and ω represent the amplitude, wave number, and angular frequency of the second sound. Here, $i = \sqrt{-1}$. According to Eq. (6), q and ω satisfy $\omega = cq/\sqrt{3}$. We calculate F under the circumstance of PSS (see Appendix C) and obtain

$$\begin{aligned} F = &-\frac{2\pi^3 a^2 T_1^2}{9\beta_0^4(\hbar c)^3 T_0^2} \sum_{n=0}^{\infty} 2(n+1) \\ &\times [V_n(qa)U_{n+1}(qa) - U_n(qa)V_{n+1}(qa)] \\ &- \frac{\pi^3 T_1^2}{5\beta_0^4(\hbar c)^3 q^2 T_0^2} \sum_{n=0}^{\infty} 2n(n+1)(n+2) \\ &\times [V_n(qa)U_{n+1}(qa) - U_n(qa)V_{n+1}(qa)], \end{aligned} \tag{10}$$

where U and V are decided by the scattering property of the second sound at the boundary of the impurity particle (see Appendix C). Then we define Y as the reduced SSRF, only related to T_1/T_0 and qa,

$$\begin{aligned} Y = \frac{F}{AE_1^{'}} = \frac{F}{\pi a^2 E_1^{'}} = &-\frac{5T_1}{3T_0} \sum_{n=0}^{\infty} 2(n+1) \\ &\times [V_n(qa)U_{n+1}(qa) - U_n(qa)V_{n+1}(qa)] \\ &- \frac{3T_1}{2T_0(qa)^2} \sum_{n=0}^{\infty} 2n(n+1)(n+2) \\ &\times [V_n(qa)U_{n+1}(qa) - U_n(qa)V_{n+1}(qa)], \end{aligned} \tag{11}$$

where A is the cross-section, and $E_1^{'}$ is the energy density of the incident second sound (see Appendix C). The physical meaning of Y is the SSRF per unit cross section and unit energy density.

The Y-qa curves are displayed in Fig. 2(a). We set the particle radius as $a = 1$ μm, and the range of q is taken as $0 \leqslant q \leqslant 10$ μm^{-1}, which is the same order as the experimental results reported in [23]. Since Y is proportional to T_1/T_0, it increases as T_1/T_0 increases. When qa increases, the second sound exchanges momentum more frequently with the particle, and Y increases monotonically. However, when qa increases further, the particle radius is much longer than the second sound wavelength, so Y remains stable as the particle is no longer sensitive to the change of the second sound wavelength. Since the value of Y is always positive for the PSS, the SSRF shows a pushing effect on the particle. Our results are in qualitative agreement with those found in acoustic waves [38].

Considering the SSRF with the ZBSS, we expect it to show distinct features as a different solution to Eq. (5). At the same time, research on the ZBSS is an intermediate case between the PSS and FBSS, suggesting that the SSRF for the ZBSS may possess common features with the cases of the PSS and FBSS. Bessel beams can be realized in acoustic fields by spiral diffraction gratings, in optical fields by holographically generated zone plates and axicons [39,40], and in thermal fields based on a similar mechanism. The ZBSS propagating along the z-axis can be described by $T_{inc} = T_0 + T_1 e^{i(q_z z - \omega t)} j_0(q_r \sqrt{x^2 + y^2})$, where q_z and q_r denote the axial and transverse wave numbers with $q_z^2 + q_r^2 = q^2$, and $j_0(x)$ is the zeroth-order Bessel function. As shown in Fig. 1(b), we use a crucial parameter, the cone-angle $\delta = \arccos(q_z/q)$, to characterize the Bessel beams. Since the Bessel beams are composed of various plane waves, δ represents the largest angle of these components relative to the z-axis. Then, we

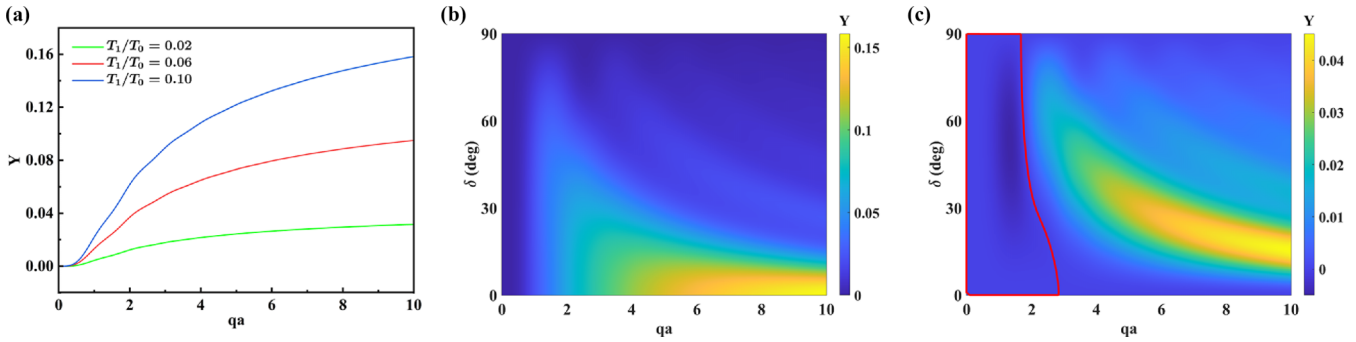

FIG. 2. Numerical results of the reduced second sound radiation force Y under the conditions of (a) plane second sound as a function of qa (where q and a are the second sound wave number and the particle radius) with the temperature ratio $T_1/T_0 = 0.02, 0.06, 0.10$ (where T_1 is the second sound amplitude, and T_0 is the background temperature); (b) zeroth-order Bessel second sound as a function of qa and δ with $T_1/T_0 = 0.10$; and (c) first-order Bessel second sound as a function of qa and δ with $T_1/T_0 = 0.10$. The area enclosed by the red line is where $Y < 0$.

obtain the reduced SSRF of the ZBSS,

$$Y = -\frac{5T_1}{3T_0}\sum_{n=0}^{\infty} 2(n+1)[V_n(qa)U_{n+1}(qa) - U_n(qa)V_{n+1}(qa)]P_n(\cos\delta)P_{n+1}(\cos\delta) - \frac{3T_1}{2T_0(qa)^2}\sum_{n=0}^{\infty} 2n(n+1)(n+2)[V_n(qa)U_{n+1}(qa) - U_n(qa)V_{n+1}(qa)]P_n(\cos\delta)P_{n+1}(\cos\delta), \quad (12)$$

where $P_n(x)$ is the nth Legendre polynomial. Figure 2(b) shows how Y varies with qa and δ, with the typical value $T_1/T_0 = 0.10$ chosen to satisfy the requirement that T_1 should be much smaller than T_0, an implicit condition for deriving Eqs. (5) and (6). Y does not increase monotonically but with some undulation as qa increases for a fixed δ (see Appendix D for more details). This phenomenon is reasonable because the Bessel second sound is composed of various plane seconds with different weights, each of which has a different angle relative to the symmetry axis. Consequently, the respective contributions of these components are different as qa increases, leading to the nonmonotony of Y after considering the total effect of these components. Nevertheless, the value of Y is always positive, indicating that the SSRF still exhibits a pushing effect on the particle. With $\delta = 0$ and $P_n(\cos\delta) = 1$, the result becomes the same as the case of the PSS. This result is reasonable since the ZBSS is reduced to the PSS when $\delta = 0$. Additionally, our results show similar features to the acoustic radiation force by the zeroth-order Bessel sound wave [38].

We finally focus on the SSRF with the FBSS. One crucial feature of the FBSS is that the temperature field does not have symmetry about the polar axis. Specifically, the expression of the FBSS has a phase factor related to the azimuthal angle. Then, we have $|u|^2 = |u_\theta|^2 + |u_\phi^2|$, which is different from the former two cases. The FBSS can be expressed as $T_{\rm inc} = T_0 + T_1 e^{i(q_z z - \omega t)} j_1(q_r\sqrt{x^2+y^2})$, where $j_1(x)$ is the first-order Bessel function. We obtain the reduced SSRF (see Appendix D),

$$Y = -\frac{5T_1}{3T_0}\sum_{n=1}^{\infty}\frac{2}{n+1}[V_n(qa)U_{n+1}(qa) - U_n(qa)V_{n+1}(qa)]P_n^1(\cos\delta)P_{n+1}^1(\cos\delta) - \frac{3T_1}{2T_0(qa)^2}\sum_{n=1}^{\infty}\frac{2n(n+2)}{n+1}[V_n(qa)U_{n+1}(qa) - U_n(qa)V_{n+1}(qa)]P_n^1(\cos\delta)P_{n+1}^1(\cos\delta), \quad (13)$$

where $P_n^m(x)$ is the associated Legendre polynomial. The variation of Y with $T_1/T_0 = 0.10$ is shown in Fig. 2(c). Unlike the former two cases, Y can be negative, indicating that the direction of the SSRF is opposite to the wave propagating direction, thus the particle can feel a pulling force. For the FBSS, the scattering state is distinct from the former two cases, with the forward scattering of the incident second sound augmented and the backward scattering suppressed [41]. The acoustic pulling force has been found in sound waves with the first-order Bessel beams [38,42–46], and the optical pulling force has been discovered in similar studies [47,48]. These results are related to the scattering state of incident waves. Additionally, the optical pulling force can be realized based on the background medium rather than the incident wave [49], and the phase shift approach has been proposed for obtaining the acoustic pulling force [50], making the acoustic pulling force more flexible than the traditional approach.

IV. DISCUSSION AND CONCLUSION

We have investigated the force impact of three distinct types of second sounds. Remarkably, there exists a thermal conduction force even in the absence of a macroscopic temperature gradient. These findings challenge the conventional notion that a nonzero temperature gradient is a prerequisite for inducing thermal conduction force. Moreover, the presence of thermal conduction force in solids demonstrates both pushing and unexpectedly pulling forces. In the case of the first-order Bessel second sound, a negative value of Y indicates the occurrence of thermal conduction pulling force. Similarly, with the higher-order Bessel second sounds (see Appendixes E,

F, and G), thermal conduction pulling force is found. When examining the second-order Bessel second sound, denoted as $T_{\rm inc} = T_0 + T_1 e^{i(q_z z-\omega t)} j_2(q_{\rm r}\sqrt{x^2+y^2})$, a negative value of Y is discovered, indicating the presence of a pulling force. This phenomenon is also revealed with the third-order and fourth-order Bessel second sounds. Hence, our physical model is both simple and effective in elucidating the essence of SSRF.

Nevertheless, we have ignored the density variation induced by the temperature in our research. Recently, a novel force has been discovered in the acoustic field, stemming from the nonuniform distribution of density, adiabatic compressibility, and dynamic viscosity within the fluid [51]. In the context of thermal conduction in solids, temperature variations can also lead to density variations. However, since our current focus is exclusively on the second sound region where the background temperature remains constant, we can disregard the density variation induced by temperature. Furthermore, we have omitted the consideration of the corresponding force effect in our analysis. Nevertheless, we anticipate that future research must give due importance to the density variation induced by temperature, similar to the case of fluids. On the other hand, our focus is on the second sound region of thermal conduction in this paper. Specifically, we consider the scenario where the relaxation times satisfy $\tau_{\rm N} \ll \tau_{\rm B} \ll \tau_{\rm R}$. Here $\tau_{\rm B}$ is the relaxation time for boundary scattering. In situations where $\tau_{\rm B} \ll \tau_{\rm N}$ and $\tau_{\rm B} \ll \tau_{\rm R}$, which is often observed in low-dimensional systems [52–54], thermal conduction occurs predominantly in the Casimir region. From a microscopic perspective, the phonons in this region exhibit ballistic behavior, allowing them to move freely over longer distances compared to other thermal conduction regimes, such as the second sound region and the diffusive region. It is worth noting that ballistic phonons also possess momentum and can interact with impurities. Drawing inspiration from the electron scattering problem, Geal derived a rough expression for the force exerted on an impurity [55]. Additionally, Richard investigated the force exerted on an atom resulting from the scattering of phonons [56]. Consequently, it is conceivable to explore the force effect in the Casimir region. This intriguing topic warrants further investigation in future studies. The other two branches of the phonon spectrum should be considered for future research, and the SSRF on a movable particle also warrants exploration. Our research could lay the groundwork for investigating the SSRF and open up the possibility of potential applications in nondestructive local conductivity tuning in crystals. Since thermal conductivity is closely related to the phonon spectrum, we can flexibly modify the vibration modes of impurity particles based on the pushing and pulling effects, thereby altering the local thermal conductivity of crystals.

To summarize, based on the wavelike characteristic of thermal conduction, we propose a basic theory for the SSRF according to the momentum conservation law for phonon systems. We focus on the SSRF with three typical wave profiles, i.e., the plane, zeroth-order Bessel, and first-order Bessel second sounds. A particle can experience a pushing effect imposed by the plane and zeroth-order Bessel second sounds. Unexpectedly, the first-order Bessel second sound can exert a pulling effect on the particle. These results can modify the local phonon spectrum in crystals at a low temperature and provide a new mechanism for local thermal conductivity manipulation.

ACKNOWLEDGMENTS

We acknowledge financial support from the National Natural Science Foundation of China under Grant No. 12035004 and the Science and Technology Commission of Shanghai Municipality under Grant No. 20JC1414700.

APPENDIX A: DYNAMIC EQUATIONS FOR β AND u

According to the local equilibrium distribution function f, we define the energy density $E(\boldsymbol{r},t)$, energy flux $\boldsymbol{Q}_{\rm i}(\boldsymbol{r},t)$, momentum density $\boldsymbol{P}_{\rm i}(\boldsymbol{r},t)$, and momentum flux $\Pi_{\rm ij}(\boldsymbol{r},t)$ of the phonon system, respectively, as follows:

$$E(\boldsymbol{r},t) = \sum_{\boldsymbol{k}} \hbar\omega_{\boldsymbol{k}} f(\boldsymbol{k},\boldsymbol{r},t), \tag{A1}$$

$$\boldsymbol{Q}_{\rm i}(\boldsymbol{r},t) = \sum_{\boldsymbol{k}} \hbar\omega_{\boldsymbol{k}} v_{\boldsymbol{k}_{\rm i}} f(\boldsymbol{k},\boldsymbol{r},t), \tag{A2}$$

$$\boldsymbol{P}_{\rm i}(\boldsymbol{r},t) = \sum_{\boldsymbol{k}} \hbar\boldsymbol{k}_{\rm i} f(\boldsymbol{k},\boldsymbol{r},t), \tag{A3}$$

$$\Pi_{\rm ij}(\boldsymbol{r},t) = \sum_{\boldsymbol{k}} \hbar\boldsymbol{k}_{\rm i} v_{\boldsymbol{k}_{\rm j}} f(\boldsymbol{k},\boldsymbol{r},t), \tag{A4}$$

where ω_k, $\boldsymbol{k}$, $\hbar$, and $\boldsymbol{v}_{k_{\rm j}} = \frac{\partial\omega_k}{\partial k_{\rm j}}$ are the phonon angular frequency, phonon wave vector, the reduced Planck constant, and the phonon group velocity, respectively. The sum is over the Brillouin zone. Since the collisions between phonons are energy-conserved and momentum-conserved, the energy and momentum conservation laws for the phonon system are

$$\frac{\partial}{\partial t}E(\boldsymbol{r},t) + \frac{\partial}{\partial \boldsymbol{r}_{\rm i}}\boldsymbol{Q}_{\rm i}(\boldsymbol{r},t) = 0, \tag{A5}$$

$$\frac{\partial}{\partial t}\boldsymbol{P}_{\rm i}(\boldsymbol{r},t) + \frac{\partial}{\partial \boldsymbol{r}_{\rm j}}\Pi_{\rm ij}(\boldsymbol{r},t) = 0. \tag{A6}$$

Equations (A5) and (A6) are the hydrodynamic equations of the phonon system. We do the Taylor expansion for f up to the first order,

$$f(\boldsymbol{k},\boldsymbol{r},t) \approx f_0 + \frac{\partial f_0}{\partial\omega_k}\left[\omega_k\frac{\beta(\boldsymbol{r},t)-\beta_0}{\beta_0} - \boldsymbol{k}\cdot\boldsymbol{u}(\boldsymbol{r},t)\right], \tag{A7}$$

where $f_0 = \frac{1}{e^{\beta_0\hbar\omega_k}-1}$ is the equilibrium distribution function at temperature T_0, i.e., the background temperature. Then, we can evaluate the results of Eqs. (A1)–(A4) by Eq. (A7). For the phonon spectrum, we use the Debye model,

$$\omega_k = c|\boldsymbol{k}|, \tag{A8}$$

where c is a constant. We consider only the contribution of one branch of lattice waves. By replacing the sums over the Brillouin zone with integrals, we can derive

$$E(\boldsymbol{r},t) = E_0 + E_1, \tag{A9a}$$

$$\boldsymbol{Q}_{\rm i}(\boldsymbol{r},t) = \frac{4}{3}\boldsymbol{u}_{\rm i}(r,t)E_0, \tag{A9b}$$

$$\boldsymbol{P}_{\rm i}(\boldsymbol{r},t) = \frac{4}{3c^2}\boldsymbol{u}_{\rm i}(r,t)E_0, \tag{A9c}$$

$$\Pi_{\rm ij}(\boldsymbol{r},t) = \frac{1}{3}\delta_{\rm ij}E(\boldsymbol{r},t), \tag{A9d}$$

where $E_0 = \frac{\pi^2}{30(\hbar c)^3\beta_0^4}$ is the energy density of the phonon system at the equilibrium state, and $E_1 = \frac{2\pi^2 T_1'}{15\beta_0^4(\hbar c)^3 T_0}$ is the energy density of the second sound; the lower indices i and j take the values x, y, and z. The Kronecker symbol δ_{ij} is equal to 1 only when i and j are identical, and 0 otherwise. T_1' is the temperature deviation from the background temperature. We denote the local temperature of the crystal by T and obtain

$$T = T_0 + T_1^{'}. \tag{A10}$$

Substituting Eqs. (A9a)–(A9d) into Eqs. (A5) and (A6) yields

$$\frac{\partial \boldsymbol{u}}{\partial t} = c^2 \nabla \frac{\beta}{\beta_0}, \tag{A11}$$

$$\frac{\partial}{\partial t}\frac{\beta}{\beta_0} = \frac{1}{3}\nabla \cdot \boldsymbol{u}. \tag{A12}$$

By combining Eqs. (A11) and (A12), we obtain the dynamic equation for β and $\boldsymbol{u}$:

$$\left(\frac{\partial^2}{\partial t^2} - \frac{c^2}{3}\nabla^2\right)\beta(r,t) = 0, \tag{A13}$$

$$\left(\frac{\partial^2}{\partial t^2} - \frac{c^2}{3}\nabla^2\right)\boldsymbol{u}_{\mathrm{i}}(r,t) = 0. \tag{A14}$$

APPENDIX B: GENERAL EXPRESSION FOR THE SSRF

We perform the Taylor expansion of f up to the second order as follows:

$$f(\boldsymbol{k},\boldsymbol{r},t) = f_0(\boldsymbol{k}) + \frac{\partial f_0(\boldsymbol{k})}{\partial \omega_k} + \frac{1}{2}\frac{\partial^2 f_0(\boldsymbol{k})}{\partial \omega_k^2}\left[\omega_k^2\left(\frac{\beta-\beta_0}{\beta_0}\right)^2 + k^2|u|^2\cos^2\theta'\right], \tag{B1}$$

where θ' is the angle between $\boldsymbol{k}$ and $\boldsymbol{u}$. Notice that

$$F = -\iint \sum_{\boldsymbol{k}} \hbar \boldsymbol{k}_{\mathrm{z}} v_{k_{\mathrm{z}}}(f - f_0)dS, \tag{B2}$$

where we have assumed the propagation direction of the second sound is along the z axis. We can substitute Eq. (B1) into Eq. (B2) to express the SSRF along the z axis as

$$F = -\frac{1}{2}\iint \sum_{\boldsymbol{k}} \hbar \boldsymbol{k}_z \boldsymbol{v}_{k_z}\frac{\partial^2 f_0(k)}{\partial \omega_{\mathrm{k}}^2}\left[\omega_k^2\left(\frac{\beta-\beta_0}{\beta_0}\right) + k^2|\boldsymbol{u}|^2\cos^2\theta'\right]dS. \tag{B3}$$

Replacing the sum with integrals, we derive

$$F = -\frac{1}{2}\iint \frac{2\pi^2}{9\beta_0^4(\hbar c)^3}\left\langle\left(\frac{\beta-\beta_0}{\beta_0}\right)^2\right\rangle + \frac{\pi^2}{15\beta_0^4\hbar^3c^5}\langle|\boldsymbol{u}|^2\rangle dS. \tag{B4}$$

Noting that

$$\frac{\beta-\beta_0}{\beta_0} = \frac{\frac{1}{T}-\frac{1}{T_0}}{\frac{1}{T_0}} = -\frac{T_1^{'}}{T} \approx -\frac{T_1^{'}}{T_0}, \tag{B5}$$

then we simplify Eq. (B4) as

$$F = -\frac{1}{2}\iint\left(\frac{2\pi^2}{9\beta_0^4(\hbar c)^3}\left\langle\left(\frac{T_1^{'}}{T_0}\right)^2\right\rangle + \frac{\pi^2}{15\beta_0^4\hbar^3c^5}\langle|u|^2\rangle\right)dS. \tag{B6}$$

Equation (B6) is the general expression of SSRF.

APPENDIX C: REDUCED SSRF FOR THE PLANE-WAVE SECOND SOUND

We need to solve the scattering field. The incident PSS along the z-axis can be expressed as

$$T_{\mathrm{inc}} = T_1\sum_{n=0}^{\infty}(2n+1)i^{\mathrm{n}}j_{\mathrm{n}}(qr)P_{\mathrm{n}}(\cos\theta)e^{-i\omega t}, \tag{C1}$$

where T_1 is the amplitude of the second sound, $j_{\mathrm{n}}(x)$ is the spherical Bessel function of order n, $P_{\mathrm{n}}(x)$ is the Legendre polynomial, θ is the polar angle, and ω is the angular frequency of the second sound. We have neglected the background temperature T_0, but this will not affect the result. The boundary of the particle is adiabatic, meaning that the radial component of the drifting velocity for the phonon system is zero at the surface of the adiabatic particle, i.e., $u_{\mathrm{r}}|_{\mathrm{r=a}} = 0$. Substituting the expression of T, i.e., Eq. (A10), into Eq. (A11) yields the following result:

$$u = \frac{c^2\nabla T_1^{'}}{i\omega T_0}. \tag{C2}$$

It can be verified that the scattering field which satisfies the adiabatic boundary condition is given by

$$T_{\mathrm{sca}} = T_1\sum_{n=0}^{\infty}(2n+1)i^{\mathrm{n}}\left[-\frac{j_{\mathrm{n}}^{'}(qa)}{h_{1,\mathrm{n}}^{'}(qa)}\right]h_{1,\mathrm{n}}(qr)P_{\mathrm{n}}(\cos\theta)e^{-i\omega t}, \tag{C3}$$

where $h_{1,\mathrm{n}}(x)$ is the spherical Hankel function of the first kind of order n, and $j_{\mathrm{n}}^{'}(x)$ and $h_{1,\mathrm{n}}^{'}(x)$ are the derivatives of $j_{\mathrm{n}}(x)$ and $h_{1,\mathrm{n}}(x)$ with respect to x, respectively. The total temperature field is given by

$$T_1^{'} = T_{\mathrm{inc}} + T_{\mathrm{sca}} = T_1\sum_{n=0}^{\infty}(2n+1)i^{\mathrm{n}} \times\left[j_{\mathrm{n}}(qr) - \frac{j_{\mathrm{n}}^{'}(qa)}{h_{1,\mathrm{n}}^{'}(qa)}h_{1,\mathrm{n}}(qr)\right]P_{\mathrm{n}}(\cos\theta)e^{-i\omega t}. \tag{C4}$$

Note that

$$h_{1,\mathrm{n}}(qr) = j_{\mathrm{n}}(qr) + in_{\mathrm{n}}(qr), \tag{C5}$$

where $n(x)$ is the spherical Bessel function of the second kind. Then Eq. (C4) can be simplified as

$$T_1^{'} = T_1\sum_{n=0}^{\infty}(2n+1)i^{\mathrm{n}}[U_{\mathrm{n}}(qr) + iV_{\mathrm{n}}(qr)]P_{\mathrm{n}}(\cos\theta)e^{-i\omega t}, \tag{C6}$$

where

$$U_{\mathrm{n}}(qr) = \mathrm{Re}\left[j_{\mathrm{n}}(qr) - \frac{j_{\mathrm{n}}^{'}(qa)}{h_{1,\mathrm{n}}^{'}(qa)} h_{1,\mathrm{n}}(qr) \right], \tag{C7}$$

$$V_{\mathrm{n}}(qr) = \mathrm{Im}\left[j_{\mathrm{n}}(qr) - \frac{j_{\mathrm{n}}^{'}(qa)}{h_{1,\mathrm{n}}^{'}(qa)} h_{1,\mathrm{n}}(qr) \right], \tag{C8}$$

where Re and Im denote the real and imaginary parts, respectively. The specific expressions of $U_{\mathrm{n}}(qr)$ and $V_{\mathrm{n}}(qr)$ are

$$U_{\mathrm{n}}(qr) = j_{\mathrm{n}}(qr) - \frac{j_{\mathrm{n}}(qa)}{j_{\mathrm{n}}^{\prime 2}(qa) + n^{\prime 2}(qa)} \times [j_{\mathrm{n}}^{'}(qa) j_{\mathrm{n}}(qr) + n_{\mathrm{n}}^{\prime}(qa) n^{\prime}(qr)], \tag{C9}$$

$$V_{\mathrm{n}}(qr) = \frac{j_{\mathrm{n}}(qa)}{j_{\mathrm{n}}^{\prime 2}(qa) + n^{\prime 2}(qa)} [j_{\mathrm{n}}(qr) n_{\mathrm{n}}^{\prime}(qa) + j_{\mathrm{n}}^{\prime}(qa) n_{\mathrm{n}}^{\prime}(qr)]. \tag{C10}$$

The following properties of the Legendre polynomial are used:

$$\int_{-1}^{1} x P_{\mathrm{n}}(x) P_{\mathrm{m+1}}(x) dx = \frac{2(n+1)}{(2n+1)(2n+3)} \delta_{\mathrm{nm}} \quad (m \geqslant n), \tag{C11}$$

$$\int_{-1}^{1} P_{\mathrm{n}}^{'} P_{\mathrm{m+1}}^{'} (1-x^2) x dx = \frac{2n(n+1)(n+2)}{(2n+1)(2n+3)} \delta_{\mathrm{nm}} \quad (m \geqslant n). \tag{C12}$$

Since the total temperature field is symmetrical about the polar axis, the total temperature field has no dependence on the azimuthal angle ϕ, indicating $\boldsymbol{u}_{\phi}|_{\mathrm{r=a}} = \mathbf{0}$. Consequently, due to $\boldsymbol{u}_{\mathrm{r}}|_{\mathrm{r=a}} = \mathbf{0}$, the SSRF expression can be reduced to

$$F = -\frac{1}{2} \iint \left(\frac{2\pi^2}{9\beta_0^4 (\hbar c)^3} \left\langle \left(\frac{T_1^{'}}{T_0} \right)^2 \right\rangle + \frac{\pi^2}{15\beta_0^4 \hbar^3 c^5} \langle |\boldsymbol{u}_{\theta}|^2 \rangle \right) dS. \tag{C13}$$

Using the equation of the time average

$$\langle R_{\mathrm{n}} R_{\mathrm{n+1}} \rangle = \tfrac{1}{2} (V_{\mathrm{n}} U_{\mathrm{n+1}} - U_{\mathrm{n}} V_{\mathrm{n+1}}), \tag{C14}$$

where

$$R_{\mathrm{n}} = \mathrm{Re}[i^{\mathrm{n}} (U_{\mathrm{n}} + i V_{\mathrm{n}}) e^{-i\omega t}], \tag{C15}$$

we obtain the result for F under the PSS as follows:

$$F = -\frac{2\pi^3 a^2 T_1^2}{9\beta_0^4 (\hbar c)^3 T_0^2} \sum_{n=0}^{\infty} 2(n+1)[V_{\mathrm{n}}(qa) U_{\mathrm{n+1}}(qa) - U_{\mathrm{n}}(qa) V_{\mathrm{n+1}}(qa)] - \frac{\pi^3 T_1^2}{5\beta_0^4 (\hbar c)^3 q^2 T_0^2} \sum_{n=0}^{\infty} 2n(n+1)(n+2)[V_{\mathrm{n}}(qa) U_{\mathrm{n+1}}(qa) - U_{\mathrm{n}}(qa) V_{\mathrm{n+1}}(qa)]. \tag{C16}$$

According to the expression of E_1, we get the energy density of the incident second sound

$$E_1^{'} = \frac{2\pi^2 T_1}{15\beta_0^4 (\hbar c)^3 T_0}. \tag{C17}$$

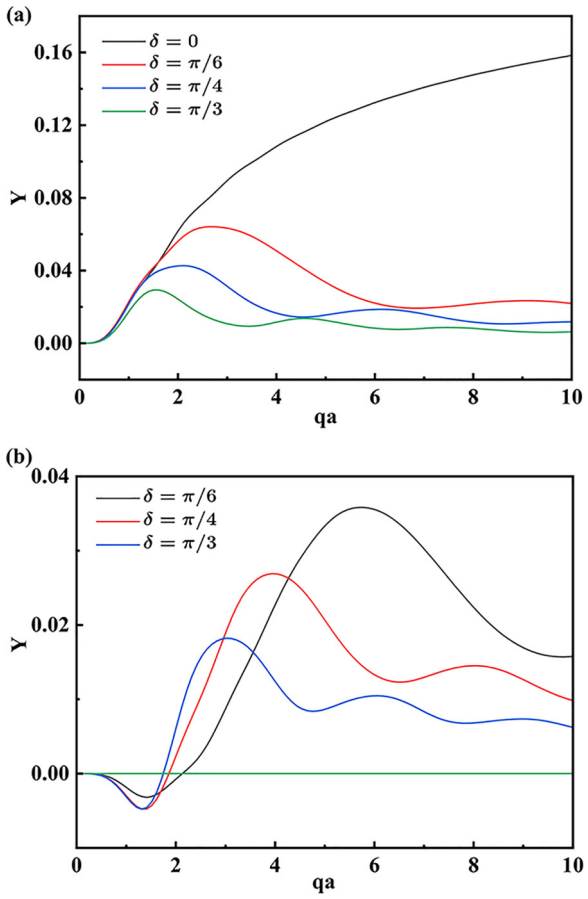

FIG. 3. Numerical simulation results of the reduced SSRF Y as a function of qa (with q and a being the wave number of the second sound and the particle radius, respectively) under the circumstance of (a) zeroth-order Bessel second sound with the cone-angle δ being $0, \pi/6, \pi/4$, and $\pi/3$, and with the temperature ratio T_1/T_0 (T_1 is the amplitude of the second sound and T_0 is the background temperature) being $T_1/T_0 = 0.1$; (b) first-order Bessel second sound with the cone-angle δ being $\pi/6, \pi/4, \pi/3$, and with the temperature ratio T_1/T_0 being $T_1/T_0 = 0.1$.

We can then calculate the following:

$$Y = -\frac{5T_1}{3T_0} \sum_{n=0}^{\infty} 2(n+1)[V_{\mathrm{n}}(qa) U_{\mathrm{n+1}}(qa) - U_{\mathrm{n}}(qa) V_{\mathrm{n+1}}(qa)] - \frac{3T_1}{2T_0 (qa)^2} \sum_{n=0}^{\infty} 2n(n+1)(n+2)[V_{\mathrm{n}}(qa) U_{\mathrm{n+1}}(qa) - U_{\mathrm{n}}(qa) V_{\mathrm{n+1}}(qa)]. \tag{C18}$$

APPENDIX D: REDUCED SSRF FOR THE FIRST-ORDER SECOND SOUND

The incident FBSS (see Fig. 3) can be expanded as

$$T_{\mathrm{inc}} = T_1 e^{-i\omega t} \sum_{n=1}^{\infty} \frac{(n-1)!}{(n+1)!} (2n+1) i^{\mathrm{n-1}} j_{\mathrm{n}}(qr) P_{\mathrm{n}}^{1}(\cos\theta) \times P_{\mathrm{n}}^{1}(\cos\delta) e^{i\phi}, \tag{D1}$$

where $P_n^1(x)$ is the associated Legendre function. With a similar procedure under the PSS circumstance, the scattering field reads

$$T_{sca} = T_1 e^{-i\omega t}\sum_{n=1}^{\infty}(2n+1)i^{n-1}\left[-\frac{j_n^{'}(qa)}{h_{1,n}^{'}(qa)}\right]h_{1,n}(qr) \times P_n^1(\cos\theta)P_n^1(\cos\delta)e^{i\phi}. \tag{D2}$$

The total temperature field can be expressed as

$$T_1^{'} = T_1 e^{-i\omega t}\sum_{n=1}^{\infty}(2n+1)i^{n-1}[U_n(qr)+iV_n(qr)]P_n^1(\cos\theta) \times P_n^1(\cos\delta)e^{i\phi}, \tag{D3}$$

where $U_n(qr)$ and $V_n(qr)$ are the same as the PSS case due to the adiabatic boundary condition. Under the FBSS circumstance, the SSRF is composed of three parts,

$$F_1 = -\frac{1}{2}\iint\frac{2\pi^2}{9\beta_0^4(\hbar c)^3}\left\langle\left(\frac{T_1^{'}}{T_0}\right)^2\right\rangle dS, \tag{D4}$$

$$F_2 = -\frac{1}{2}\iint\frac{\pi^2}{15\beta_0^4\hbar^3c^5}\langle|\boldsymbol{u}_\theta|^2\rangle dS, \tag{D5}$$

$$F_3 = -\frac{1}{2}\iint\frac{\pi^2}{15\beta_0^4\hbar^3c^5}\langle|\boldsymbol{u}_\phi|^2\rangle dS. \tag{D6}$$

The following properties of the Legendre polynomial and the associated Legendre polynomial are used:

$$(2n+1)xP_n(x) = (n+1)P_{n+1}(x) + nP_{n-1}(x), \tag{D7a}$$

$$nP_n(x) = xP_n^{'}(x) - P_{n-1}^{'}(x), \tag{D7b}$$

$$(n+1)P_n(x) = P_{n+1}^{'}(x) - xP_n^{'}(x), \tag{D7c}$$

$$(2n+1)P_n(x) = P_{n+1}^{'}(x) - P_{n-1}^{'}(x), \tag{D7d}$$

$$(1-x^2)P_n^{'}(x) = nP_{n-1}(x) - nxP_n(x), \tag{D7e}$$

$$(2n+1)xP_n^m(x) = (n+m)P_{n-1}^m(x) + (l+1-m) \times P_{n+1}^m(x) \quad (m \geqslant 0), \tag{D8a}$$

$$(2n+1)(1-x^2)\frac{dP_n^m}{dx} = (n+1)(n+m)P_{n-1}^m(x) - n(n+1-m)P_{n+1}^m(x) \quad (m \geqslant 0). \tag{D8b}$$

Differentiating both sides of Eq. (D8a) with respect to x, we obtain

$$xP_n^{m'}(x) = \frac{(n+m)P_{n-1}^{m'}(x) + (n+1-m)P_{n+1}^{m'}(x)}{2n+1} - P_n^m(x). \tag{D9}$$

Differentiating the both sides of Eq. (D7c) with respect to x, we get

$$xP_n^{''}(x) = P_{n+1}^{''}(x) - (n+2)P_n^{'}(x). \tag{D10}$$

By performing similar operations, we obtain the following equations:

$$xP_n^{'''}(x) = P_{n+1}^{'''}(x) - (n+3)P_n^{''}(x), \tag{D11a}$$

$$xP_n^{''''}(x) = P_{n+1}^{''''}(x) - (n+4)P_n^{'''}(x). \tag{D11b}$$

By combining Eqs. (D7a) and (D7e), we have

$$(1-x^2)P_n^{'}(x) = \frac{n(n+1)[P_{n-1}(x) - P_{n+1}(x)]}{(2n+1)}. \tag{D12}$$

Differentiating both sides of Eq. (D12) with respect to x and combining it with Eq. (D7d) yields

$$(1-x^2)P_n^{''}(x) = 2xP_n^{'}(x) - n(n+1)P_n(x). \tag{D13}$$

Combining Eq. (D7c), we get

$$(1-x^2)P_n^{''}(x) = 2P_{n+1}^{'}(x) - (n+1)(n+2)P_n(x). \tag{D14}$$

By performing similar operations and combining Eqs. (D10), (D11a), and (D11b), we find

$$(1-x^2)P_n^{'''}(x) = 4P_{n+1}^{''}(x) - (n+2)(n+3)P_n^{'}(x), \tag{D15a}$$

$$(1-x^2)P_n^{''''}(x) = 6P_{n+1}^{'''}(x) - (n+3)(n+4)P_n^{''}(x), \tag{D15b}$$

$$(1-x^2)P_n^{'''''}(x) = 8P_{n+1}^{''''}(x) - (n+4)(n+5)P_n^{'''}(x). \tag{D15c}$$

Given $P_n(1) = 1$ and $P_n(-1) = (-1)^n$, with Eq. (D14) and Eqs. (D15a)–(D15c), we obtain the following:

$$P_n^{'}(1) = \tfrac{1}{2}n(n+1), \tag{D16a}$$

$$P_n^{'}(-1) = \tfrac{1}{2}n(n+1)(-1)^{n-1}, \tag{D16b}$$

$$P_n^{''}(1) = \tfrac{1}{8}(n-1)n(n+1)(n+2), \tag{D16c}$$

$$P_n^{''}(-1) = \tfrac{1}{8}(n-1)n(n+1)(n+2)(-1)^{n-2}, \tag{D16d}$$

$$P_n^{'''}(1) = \tfrac{1}{48}(n-2)n(n+1)(n+2)(n+3), \tag{D16e}$$

$$P_n^{'''}(-1) = \tfrac{1}{48}(n-2)(n-1)n(n+1)(n+2)(n+3)(-1)^{n-3}, \tag{D16f}$$

$$P_n^{''''}(1) = \tfrac{1}{384}(n-3)(n-2)n(n+1)(n+2)(n+3)(n+4), \tag{D16g}$$

$$P_n^{''''}(-1) = \tfrac{1}{384}(n-3)(n-2)(n-1)n(n+1)(n+2) \times (n+3)(n+4)(-1)^{n-4}. \tag{D16h}$$

Then we have

$$\int_{-1}^{1}P_n^{'2}(x)dx = \int_{-1}^{1}P_n^{'}(x)dP_n(x) = P_n^{'}(x)P_n(x)|_{-1}^{1} - \int_{-1}^{1}P_n(x)P_n^{''}(x)dx. \tag{D17}$$

Noting that

$$
\begin{aligned}
-\int_{-1}^{1} P_{\mathrm{n}}(x)P_{\mathrm{n}}^{''}(x)dx &= -\frac{1}{2^{2\mathrm{n}}(n!)^2}\int_{-1}^{1}\frac{d^{\mathrm{n}}}{dx^{\mathrm{n}}}(x^2-1)^{\mathrm{n}}\frac{d^{\mathrm{n}+2}}{dx^{\mathrm{n}+2}}(x^2-1)^{\mathrm{n}}dx \\
&= -\frac{1}{2^{2\mathrm{n}}(n!)^2}\int_{-1}^{1}\frac{d^{\mathrm{n}+2}}{dx^{\mathrm{n}+2}}(x^2-1)^{\mathrm{n}}d\left[\frac{d^{\mathrm{n}-1}}{dx^{\mathrm{n}-1}}(x^2-1)^{\mathrm{n}}\right] \\
&= \frac{-1}{2^{2\mathrm{n}}(n!)^2}\left[\frac{d^{\mathrm{n}+2}}{dx^{\mathrm{n}+2}}(x^2-1)^{\mathrm{n}}\frac{d^{\mathrm{n}-1}}{dx^{\mathrm{n}-1}}(x^2-1)^{\mathrm{n}}|_{-1}^{1} - \int_{-1}^{1}\frac{d^{\mathrm{n}-1}}{dx^{\mathrm{n}-1}}(x^2-1)^{\mathrm{n}}\frac{d^{\mathrm{n}+3}}{dx^{\mathrm{n}+3}}(x^2-1)^{\mathrm{n}}dx\right] \\
&= \frac{(-1)^2}{2^{2\mathrm{n}}(n!)^2}\int_{-1}^{1}\frac{d^{\mathrm{n}+3}}{dx^{\mathrm{n}+3}}(x^2-1)^{\mathrm{n}}d\left[\frac{d^{\mathrm{n}-2}}{dx^{\mathrm{n}-2}}(x^2-1)^{\mathrm{n}}\right] \\
&= \cdots = \frac{(-1)^{\mathrm{n}-1}}{2^{2\mathrm{n}}(n!)^2}\int_{-1}^{1}\frac{d^{2\mathrm{n}}}{dx^{2\mathrm{n}}}(x^2-1)^{\mathrm{n}}d\left[\frac{d}{dx}(x^2-1)^{\mathrm{n}}\right] = \frac{(-1)^{\mathrm{n}-1}}{2^{2\mathrm{n}}(n!)^2}(2n)!\frac{d}{dx}(x^2-1)^{\mathrm{n}}|_{-1}^{1} = 0,
\end{aligned}
\tag{D18}
$$

combining Eqs. (D16a) and (D16b) yields

$$
\int_{-1}^{1} P_{\mathrm{n}}^{'2}(x)dx = n(n+1). \tag{D19}
$$

Combining Eq. (D7c), we get

$$
\int_{-1}^{1} P_{\mathrm{n}}(x)P_{\mathrm{n}+1}^{'}(x)dx = \int_{-1}^{1} P_{\mathrm{n}}(x)[(n+1)P_{\mathrm{n}}(x) + xP_{\mathrm{n}}^{'}(x)]dx = \int_{-1}^{1}(n+1)P_{\mathrm{n}}^{2}(x) + xP_{\mathrm{n}}^{'}(x)P_{\mathrm{n}}(x)dx = 2. \tag{D20}
$$

Combining Eq. (D7d), we obtain

$$
\int_{-1}^{1} P_{\mathrm{n}}^{'}(x)P_{\mathrm{n}+1}(x)dx = \int_{-1}^{1} P_{\mathrm{n}+1}(x)[P_{\mathrm{n}+2}^{'}(x) - (2n+3)P_{\mathrm{n}+1}(x)]dx = 2 - 2 = 0. \tag{D21}
$$

By combining Eqs. (D16a)–(D16f), we find

$$
\int_{-1}^{1} P_{\mathrm{n}}^{''2}(x)dx = \int_{-1}^{1} P_{\mathrm{n}}^{''}(x)dP_{\mathrm{n}}^{'}(x) = P_{\mathrm{n}}^{'}(x)P_{\mathrm{n}}^{''}(x)|_{-1}^{1} - \int_{-1}^{1} P_{\mathrm{n}}^{'}(x)P_{\mathrm{n}}^{'''}(x)dx = \frac{(n^2+n+3)(n-1)n(n+1)(n+2)}{12} \tag{D22}
$$

and

$$
\int_{-1}^{1} P_{\mathrm{n}}^{'}(x)P_{\mathrm{n}}^{'''}(x)dx = \frac{(n-2)(n-1)n(n+1)(n+2)(n+3)}{24}. \tag{D23}
$$

Combining Eqs. (D10) and (D19), we have

$$
\int_{-1}^{1} P_{\mathrm{n}}^{'}(x)P_{\mathrm{n}+1}^{''}(x)dx = \frac{n(n+1)(n+2)(n+3)}{4}. \tag{D24}
$$

Combining Eqs. (D7d), (D18), and (D24) yields

$$
\int_{-1}^{1} P_{\mathrm{n}}^{''}(x)P_{\mathrm{n}+1}^{'}(x)dx = \int_{-1}^{1} P_{\mathrm{n}}{''}(x)[(2n+1)P_{\mathrm{n}}(x) + P_{\mathrm{n}-1}^{'}(x)] = \frac{(n-1)n(n+1)(n+2)}{4}. \tag{D25}
$$

Combining Eqs. (D11a) and (D22), we get

$$
\int_{-1}^{1} P_{\mathrm{n}}^{''}(x)P_{\mathrm{n}+1}^{'''}(x)dx = \frac{(3n^2+n+10)(n-1)n(n+1)(n+2)(n+3)(n+4)}{192}. \tag{D26}
$$

Combining Eqs. (D7d) and (D26), we find

$$
\int_{-1}^{1} P_{\mathrm{n}}^{''}(x)P_{\mathrm{n}-1}^{'''}(x)dx = \frac{(3n^2+5n+12)(n-3)(n-2)(n-1)n(n+1)(n+2)}{192}. \tag{D27}
$$

Thus, we obtain

$$
\int_{-1}^{1} P_{\mathrm{n}-1}(x)P_{\mathrm{n}+3}^{''}(x)dx = \int_{-1}^{1} P_{\mathrm{n}-1}(x)[(2n+5)P_{\mathrm{n}+2}^{'}(x) + P_{\mathrm{n}+1}^{''}(x)]dx = 4(2n+3), \tag{D28a}
$$

$$
\int_{-1}^{1} P_{\mathrm{n}-1}^{'}(x)P_{\mathrm{n}+3}^{'}(x)dx = \int_{-1}^{1} [P_{\mathrm{n}+1}^{'}(x) - (2n+1)P_{\mathrm{n}}(x)][(2n+5)P_{\mathrm{n}+2}(x) + P_{\mathrm{n}+1}^{'}(x)]dx = n(n-1), \tag{D28b}
$$

$$\int_{-1}^{1} P_{n+1}^{'''}(x)P_{n+2}(x)dx = \int_{-1}^{1} P_{n+2}(x)dP_{n+1}^{''}(x) = P_{n+1}^{''}(x)P_{n+2}(x)|_{-1}^{1} - \int_{-1}^{1} P_{n+2}^{'}(x)P_{n+1}^{''}(x) = 0, \tag{D28c}$$

$$\int_{-1}^{1} P_{n}^{''}(x)P_{n+2}(x)dx = \int_{-1}^{1} [P_{n+2}^{''}(x) - (2n+3)P_{n+1}^{'}(x)]P_{n+2}(x)dx = 0, \tag{D28d}$$

$$\int_{-1}^{1} P_{n-1}(x)P_{n+2}^{'}(x)dx = \int_{-1}^{1} P_{n-1}(x)[(2n+3)P_{n+1}(x) + P_{n}^{'}(x)]dx = 2, \tag{D28e}$$

$$\int_{-1}^{1} P_{n-1}(x)P_{n+1}^{'}(x)dx = \int_{-1}^{1} P_{n-1}(x)[(2n+1)P_{n}^{'}(x) + P_{n-1}^{''}(x)]dx = 2(2n+1), \tag{D28f}$$

$$\int_{-1}^{1} P_{n+1}^{'}(x)P_{n+3}^{'''}(x)dx = \int_{-1}^{1} P_{n+1}^{'}(x)[(2n+5)P_{n+2}^{''}(x) + P_{n+1}^{'''}(x)]dx = \frac{n(n+1)(n+2)(n+3)(n+4)(n+5)}{12}, \tag{D28g}$$

$$\int_{-1}^{1} P_{n}^{'}(x)P_{n+3}^{''}(x)dx = \int_{-1}^{1} P_{n}^{'}(x)[(2n+5)P_{n+2}^{'}(x) + P_{n+1}^{''}(x)]dx = \frac{n(n+1)(n^2+13n+26)}{4}, \tag{D28h}$$

$$\int_{-1}^{1} P_{n+2}^{'}(x)P_{n}^{'}(x)dx = \int_{-1}^{1} P_{n}^{'}(x)[(2n+3)P_{n+1}(x) + P_{n}^{'}(x)]dx = n(n+1), \tag{D28i}$$

$$\int_{-1}^{1} P_{n+2}^{''}(x)P_{n}(x)dx = \int_{-1}^{1} P_{n}(x)[(2n+3)P_{n+1}^{'}(x) + P_{n}^{''}(x)]dx = 2(2n+3), \tag{D28j}$$

$$\int_{-1}^{1} P_{n+2}^{''}(x)P_{n}(x)dx = \int_{-1}^{1} P_{n}(x)[(2n+3)P_{n+1}^{'}(x) + P_{n}^{''}(x)]dx = 2(2n+3), \tag{D28k}$$

$$\int_{-1}^{1} P_{n+2}^{''}(x)P_{n-1}^{'}(x)dx = \int_{-1}^{1} [(2n+3)P_{n+1}^{'}(x) + P_{n}^{''}(x)][P_{n+1}^{'}(x) - (2n+1)P_{n}(x)]dx = \frac{(n-1)n(n^2+11n+14)}{4}, \tag{D28l}$$

$$\int_{-1}^{1} P_{n+1}^{'''}(x)P_{n+3}^{'}(x)dx = \int_{-1}^{1} P_{n+1}^{'''}(x)[(2n+5)P_{n+2}(x) + P_{n+1}^{'}(x)]dx = \frac{(n-1)n(n+1)(n+2)(n+3)(n+4)}{24}, \tag{D28m}$$

$$\int_{-1}^{1} P_{n+1}^{'''}(x)P_{n+2}(x)dx = P_{n+1}^{''}(x)P_{n+2}(x)|_{-1}^{1} - \int_{-1}^{1} P_{n+1}^{''}(x)P_{n+2}^{'}(x)dx = 0, \tag{D28n}$$

$$\int_{-1}^{1} P_{n}^{''}(x)P_{n+3}^{'}(x)dx = \int_{-1}^{1} [P_{n+2}^{''}(x) - (2n+3)P_{n+1}^{'}(x)][(2n+5)P_{n+2}(x) + P_{n+1}^{'}(x)]dx = \frac{(n-1)n(n+1)(n+2)}{4}, \tag{D28o}$$

$$\begin{aligned}\int_{-1}^{1} P_{n+1}^{'''}(x)P_{n+4}^{''}(x)dx &= \int_{-1}^{1} [P_{n+3}^{'''}(x) - (2n+5)P_{n+2}^{''}(x)][(2n+7)P_{n+3}^{'}(x) + P_{n+2}^{''}(x)]dx \\ &= \frac{(3n^4+30n^3+57n^2-90n)[(n+1)(n+2)(n+3)(n+4)]}{192},\end{aligned} \tag{D28p}$$

$$\begin{aligned}\int_{-1}^{1} P_{n}^{''}(x)P_{n+4}^{''}(x)dx &= \int_{-1}^{1} [P_{n+2}^{''}(x) - (2n+3)P_{n+1}^{'}(x)][(2n+7)[(2n+5)P_{n+2}(x) + P_{n+1}{}^{'}(x)] + P_{n+2}^{''}(x)]dx \\ &= \frac{(n+1)(n+2)(n^4+12n^3+20n-33n)}{12},\end{aligned} \tag{D28q}$$

$$\begin{aligned}\int_{-1}^{1} P_{n-1}^{'}(x)P_{n+4}^{''}(x)dx &= \int_{-1}^{1} [P_{n+1}^{'}(x) - (2n+1)P_{n}(x)]\{(2n+7)[(2n+5)P_{n+2}(x) + P_{n+1}^{'}(x)] + P_{n+2}^{''}\}dx \\ &= \frac{(n^4+18n^3+23n^2-42n)}{4}.\end{aligned} \tag{D28r}$$

Now, our main task is to evaluate the following three expressions: $C1 = \int_{-1}^{1} P_{n}^{1}(x)P_{n+1}^{1}(x)xdx$; $C2 = \int_{-1}^{1} P_{n}^{1}(x)P_{n+1}^{1}(x)\frac{x}{1-x^2}dx$; and $C3 = \int_{-1}^{1} x(1-x^2)P_{n}^{1'}(x)P_{n+1}^{1'}(x)dx$. Note that

$$\int_{-1}^{1} P_{n}^{1}(x)P_{n+1}^{1}(x)xdx = \int_{-1}^{1} P_{n}^{'}(x)P_{n+1}^{'}(x)x(1-x^2) = \frac{2n(n+1)(n+2)}{(2n+1)(2n+3)}, \tag{D29}$$

$$\begin{aligned}\int_{-1}^{1} P_{n}^{1}(x)P_{n+1}^{1}(x)\frac{x}{1-x^2}dx &= \int_{-1}^{1} xP_{n}^{'}(x)P_{n+1}^{'}(x)dx = \int_{-1}^{1} [P_{n+1}^{'}(x) - (n+1)P_{n}(x)]P_{n+1}^{'}(x)dx \\ &= n(n+1).\end{aligned} \tag{D30}$$

To evaluate $\int_{-1}^{1} x(1-x^2)P_{\rm n}^{1'}(x)P_{\rm n+1}^{1'}(x)dx$, we know that

$$\int_{-1}^{1} P_{\rm n}^{1'}(x)P_{\rm n+1}^{1'}(x)(1-x^2)xdx = \int_{-1}^{1}\left[\frac{(n+1)P_{\rm n-1}^{1'}(x)+nP_{\rm n+1}^{1'}(x)}{2n+1}-P_{\rm n}^{1}\right]\left[\frac{(n+2)^2P_{\rm n}^{1}(x)-(n+1)^2P_{\rm n+2}^{1}(x)}{2n+3}\right]dx, \tag{D31}$$

and

$$\int_{-1}^{1} P_{\rm n-1}^{1'}(x)P_{\rm n}^{1}(x)dx = \int_{-1}^{1}[P_{\rm n-1}^{''}(x)(1-x^2)^{\frac{1}{2}}-\frac{x}{(1-x^2)^{\frac{1}{2}}}](1-x^2)^{\frac{1}{2}}P_{\rm n}^{'}(x)dx = n(n+1)-2n = -n(n-1), \tag{D32}$$

$$\int_{-1}^{1} P_{\rm n-1}^{1'}(x)P_{\rm n+2}^{1}(x)dx = \int_{-1}^{1}(1-x^2)P_{\rm n-1}^{''}(x)P_{\rm n+2}^{'}(x)-xP_{\rm n-1}^{'}(x)P_{\rm n+2}^{'}(x)dx = -n(n-1), \tag{D33}$$

$$\int_{-1}^{1} P_{\rm n+1}^{1'}(x)P_{\rm n+2}^{1}(x)dx = \int_{-1}^{1}(1-x^2)P_{\rm n+1}^{''}(x)P_{\rm n+2}^{'}(x)-xP_{\rm n+1}^{'}(x)P_{\rm n+2}^{'}(x)dx = -(n+1)(n+2), \tag{D34}$$

$$\int_{-1}^{1} P_{\rm n+1}^{1'}(x)P_{\rm n}^{1}(x)dx = \int_{-1}^{1}(1-x^2)P_{\rm n+1}^{''}(x)P_{\rm n}^{'}(x)-xP_{\rm n+1}^{'}(x)P_{\rm n}^{'}(x)dx = n(n+1). \tag{D35}$$

Then we have

$$\int_{-1}^{1} P_{\rm n}^{1'}(x)P_{\rm n+1}^{1'}(x)(1-x^2)xdx = \frac{n(n+1)(2n^3+4n-3)}{(2n+1)(2n+3)}. \tag{D36}$$

For an mth-order Bessel second sound, the SSRF is given by

$$\begin{aligned} F = &-\frac{2\pi^3a^2T_1^2}{9\beta_0^4(\hbar c)^3T_0^2}\sum_{n=m}^{\infty}C1\frac{(n-m)!(n+1-m)!(2n+1)(2n+3)}{(n+m)!(n+1+m)!}[V_{\rm n}(qa)U_{\rm n+1}(qa)-U_{\rm n}(qa)V_{\rm n+1}(qa)]P_{\rm n}^{\rm m}(\cos\delta)P_{\rm n+1}^{\rm m}(\cos\delta)\\ &-\frac{\pi^3T_1^2}{5\beta_0^4(\hbar c)^3q^2T_0^2}\sum_{n=m}^{\infty}(m^2C2+C3)\frac{(n-m)!(n+1-m)!(2n+1)(2n+3)}{(n+m)!(n+1+m)!}\\ &\times[V_{\rm n}(qa)U_{\rm n+1}(qa)-U_{\rm n}(qa)V_{\rm n+1}(qa)]P_{\rm n}^{\rm m}(\cos\delta)P_{\rm n+1}^{\rm m}(\cos\delta), \end{aligned} \tag{D37}$$

and the reduced SSRF is

$$\begin{aligned} Y = &-\frac{5T_1}{3T_0}\sum_{n=m}^{\infty}C1\frac{(n-m)!(n+1-m)!(2n+1)(2n+3)}{(n+m)!(n+1+m)!}[V_{\rm n}(qa)U_{\rm n+1}(qa)-U_{\rm n}(qa)V_{\rm n+1}(qa)]P_{\rm n}^{\rm m}(\cos\delta)P_{\rm n+1}^{\rm m}(\cos\delta)\\ &-\frac{3T_1}{2T_0(qa)^2}\sum_{n=m}^{\infty}(m^2C2+C3)\frac{(n-m)!(n+1-m)!(2n+1)(2n+3)}{(n+m)!(n+1+m)!}\\ &\times[V_{\rm n}(qa)U_{\rm n+1}(qa)-U_{\rm n}(qa)V_{\rm n+1}(qa)]P_{\rm n}^{\rm m}(\cos\delta)P_{\rm n+1}^{\rm m}(\cos\delta). \end{aligned} \tag{D38}$$

In the case of FBSS, then, we see

$$\int_{-1}^{1} P_{\rm n}^{1'}(x)P_{\rm n+1}^{1'}(x)(1-x^2)xdx+\int_{-1}^{1}P_{\rm n}^{1}(x)P_{\rm n+1}^{1}(x)\frac{x}{1-x^2}dx = \frac{2n^2(n+1)(n+2)^2}{(2n+1)(2n+3)}. \tag{D39}$$

Thus, we obtain the following expression for Y:

$$\begin{aligned} Y = &-\frac{5T_1}{3T_0}\sum_{n=1}^{\infty}\frac{2}{n+1}[V_{\rm n}(qa)U_{\rm n+1}(qa)-U_{\rm n}(qa)V_{\rm n+1}(qa)]P_{\rm n}^{1}(\cos\delta)P_{\rm n+1}^{1}(\cos\delta)\\ &-\frac{3T_1}{2T_0(qa)^2}\sum_{n=1}^{\infty}\frac{2n(n+2)}{n+1}[V_{\rm n}(qa)U_{\rm n+1}(qa)-U_{\rm n}(qa)V_{\rm n+1}(qa)]P_{\rm n}^{1}(\cos\delta)P_{\rm n+1}^{1}(\cos\delta). \end{aligned} \tag{D40}$$

APPENDIX E: REDUCED SSRF FOR THE SECOND-ORDER BESSEL SECOND SOUND

To calculate the reduced SSRF of the second-order Bessel second sound (see Fig. 4), the following expressions must be evaluated : $C1=\int_{-1}^{1}P_{\rm n}^{2}(x)P_{\rm n+1}^{2}(x)xdx$, $C2=\int_{-1}^{1}P_{\rm n}^{2}(x)P_{\rm n+1}^{2}(x)\frac{x}{1-x^2}dx$, and $C3=\int_{-1}^{1}x(1-x^2)P_{\rm n}^{2'}(x)P_{\rm n+1}^{2'}(x)dx$. Noting that

$$\int_{-1}^{1}xP_{\rm n}^{2}(x)P_{\rm n+1}^{2}(x)dx = \frac{n-1}{2n+1}\frac{2}{2n+3}\frac{(n+3)!}{(n-1)!}, \tag{E1}$$

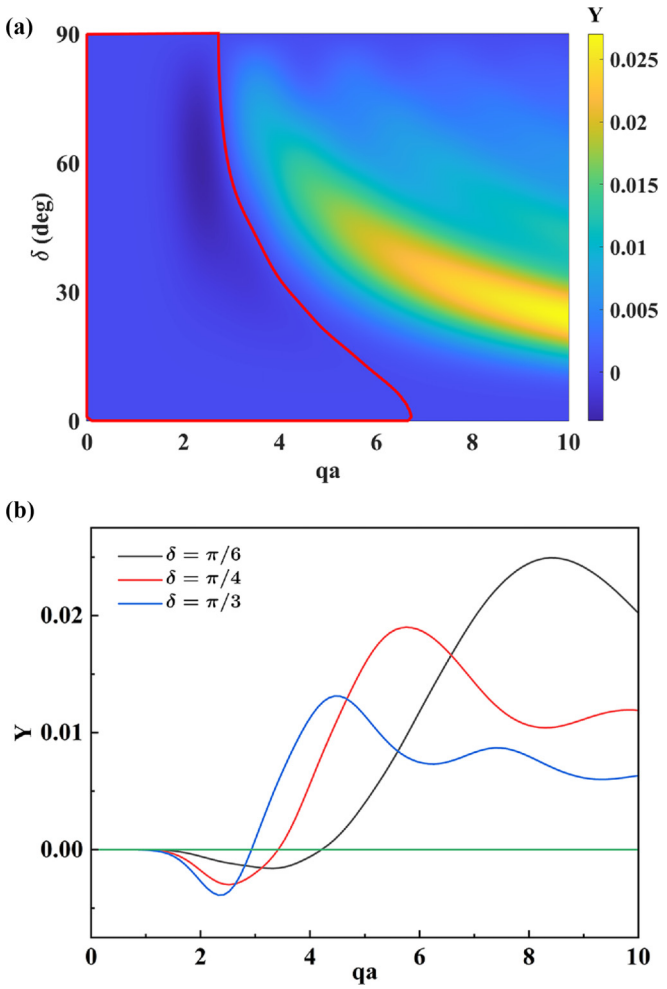

FIG. 4. Numerical simulation results of the reduced SSRF Y under the circumstance of the second-order Bessel second sound (a) as a function of both qa and δ (the area enclosed by the red line is where $Y < 0$); and (b) as function of qa with the cone-angle δ being $\pi/6$, $\pi/4$, $\pi/3$, and with the temperature ratio T_1/T_0 being $T_1/T_0 = 0.10$.

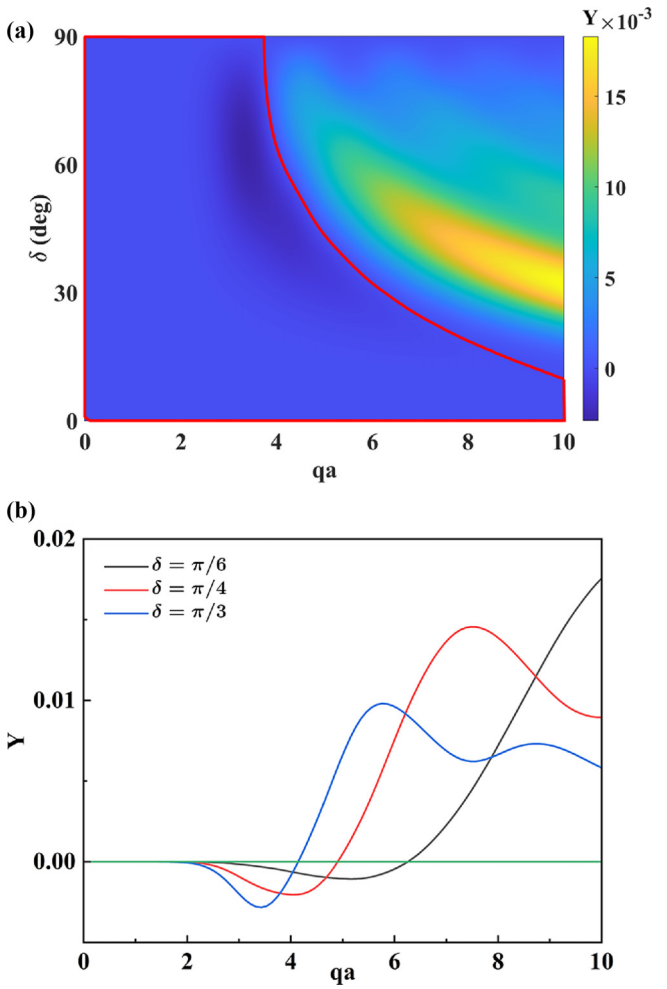

FIG. 5. Numerical simulation results of the reduced SSRF Y under the circumstance of the third-order Bessel second sound (a) as a function of both qa and δ (the area enclosed by the red line is where $Y < 0$); and (b) as a function of qa with the cone-angle δ being $\pi/6$, $\pi/4$, $\pi/3$, and with the temperature ratio T_1/T_0 being $T_1/T_0 = 0.10$.

$$\int_{-1}^{1}(1-x^2)xP_n^{2'}(x)P_{n+1}^{2'}(x)dx = \int_{-1}^{1}\left[\frac{(n+2)P_{n-1}^{2'}(x)+(n-1)P_{n+1}^{2'}(x)}{2n+1}-P_n^2(x)\right] \times\left[\frac{(n+2)(n+3)}{2n+3}P_n^2(x)-\frac{n(n+1)}{2n+3}P_{n+2}^2(x)\right]dx, \quad \text{(E2)}$$

and

$$\int_{-1}^{1}P_{n-1}^{2'}(x)P_n^2(x)dx = \int_{-1}^{1}[2P_n''(x)-n(n+1)P_{n-1}'(x)] \times[2P_{n+1}'(x)-(n+1)(n+2)P_n(x)]dx = -(n-2)(n-1)n(n+1), \quad \text{(E3)}$$

$$\int_{-1}^{1}P_n^{2'}(x)P_{n-1}^2(x)dx = \int_{-1}^{1}P_{n-1}^2(x)dP_n^2(x) = P_n^2(x)P_{n-1}^2(x)|_{-1}^{1} - \int_{-1}^{1}P_n^2(x)dP_{n-1}^2(x) = -\int_{-1}^{1}P_{n-1}^{2'}P_n^2(x)dx = -(n-2) \times(n-1)n(n+1), \quad \text{(E4)}$$

thus we find

$$\int_{-1}^{1}P_n^2(x)P_{n+1}^{2'}(x)dx = (n-1)n(n+1)(n+2), \quad \text{(E5)}$$

$$\int_{-1}^{1}P_{n+1}^{2'}(x)P_{n+2}^2(x)dx = -n(n+1)(n+2)(n+3). \quad \text{(E6)}$$

Remembering that

$$\int_{-1}^{1}P_n^{2^2}(x)dx = \frac{(n+2)!}{(n-2)!}\frac{2}{2n+1} = \frac{1}{2n+1}(n-1)n(n+1)(n+2) \quad \text{(E7)}$$

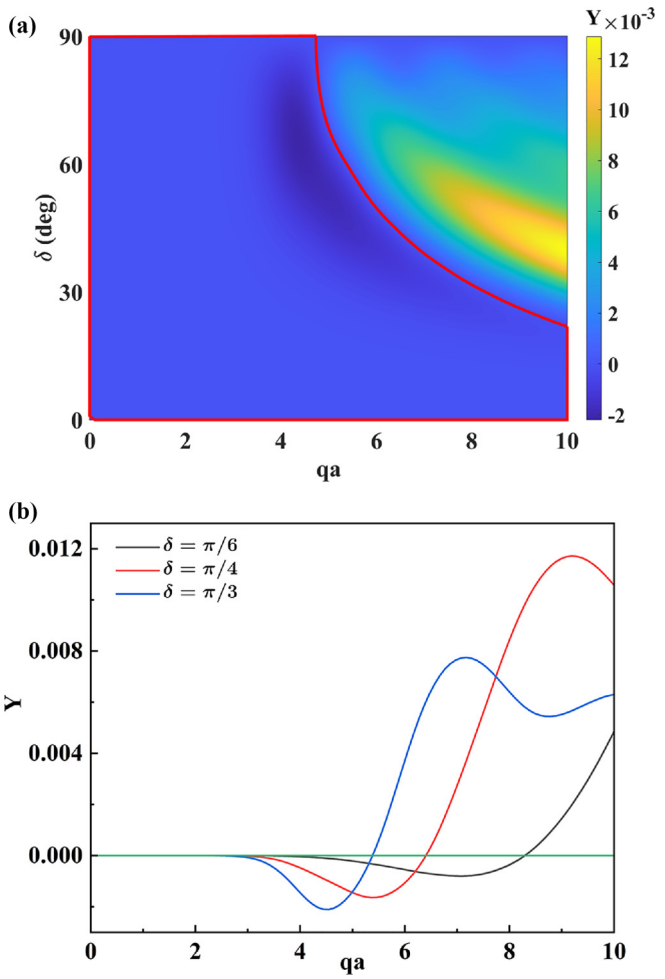

FIG. 6. Numerical simulation results of the reduced SSRF Y under the circumstance of the fourth-order Bessel second sound (a) as a function of both qa and δ (the area enclosed by the red line is where $Y < 0$); and (b) as a function of qa with the cone-angle δ being $\pi/6$, $\pi/4$, $\pi/3$, and with the temperature ratio T_1/T_0 being $T_1/T_0 = 0.10$.

and

$$\int_{-1}^{1} P_{n-1}^{2'}(x)P_{n+2}^{2}(x)dx = \int_{-1}^{1}[2P_n''(x) - n(n+1)P_{n-1}'(x)] \times [2P_{n+3}'(x) - (n+3)(n+4)P_n(x)]dx = -(n-2)(n-1)n(n+1), \quad \text{(E8)}$$

therefore we have

$$\int_{-1}^{1}(1-x^2)xP_n^{2'}(x)P_{n+1}^{2'}(x)dx = \frac{(n-1)n(n+1)(n+2)[2n^3+2n^2-4n-6]}{(2n+1)(2n+3)} \quad \text{(E9)}$$

and

$$\int_{-1}^{1}P_n^2(x)P_{n+1}^2(x)\frac{x}{1-x^2}dx = \int_{-1}^{1}(1-x^2)xP_n''(x)P_{n+1}''(x) = \frac{(n-1)n(n+1)(n+2)}{2}. \quad \text{(E10)}$$

Thus, we can get

$$\int_{-1}^{1}(1-x^2)xP_n^{2'}(x)P_{n+1}^{2'}(x)dx + 4\int_{-1}^{1}P_n^2(x)P_{n+1}^2(x)\frac{x}{1-x^2}dx = \frac{(n-1)n(n+1)(n+2)(2n^3+10n^2+12n)}{(2n+1)(2n+3)}. \quad \text{(E11)}$$

Then, the results of Y can be expressed as

$$Y = -\frac{5T_1}{3T_0}\sum_{n=2}^{\infty}\frac{2}{n(n+1)(n+2)}[V_n(qa)U_{n+1}(qa) - U_n(qa)V_{n+1}(qa)]P_n^2(\cos\delta)P_{n+1}^2(\cos\delta) - \frac{3T_1}{2T_0(qa)^2}\sum_{n=2}^{\infty}\frac{2}{n+1}[V_n(qa)U_{n+1}(qa) - U_n(qa)V_{n+1}(qa)]P_n^2(\cos\delta)P_{n+1}^2(\cos\delta). \quad \text{(E12)}$$

APPENDIX F: REDUCED SSRF FOR THE THIRD-ORDER BESSEL SECOND SOUND

Similarly, the third-order Bessel second sound should be evaluated in terms of the following expressions: $C1 = \int_{-1}^{1}P_n^3(x)P_{n+1}^3(x)xdx$, $C2 = \int_{-1}^{1}P_n^3(x)P_{n+1}^3(x)\frac{x}{1-x^2}dx$, and $C3 = \int_{-1}^{1}x(1-x^2)P_n^{3'}(x)(x)P_{n+1}^{3'}(x)dx$. Noting that

$$\int_{-1}^{1}xP_n^3(x)P_{n+1}^3(x)dx = \frac{n-2}{2n+1}\frac{2}{2n+3}\frac{(n+4)!}{(n-2)!}, \quad \text{(F1)}$$

$$\int_{-1}^{1}P_n^3(x)P_{n+1}^3(x)\frac{x}{1-x^2}dx = \int_{-1}^{1}(1-x^2)^2xP_n'''(x)P_{n+1}'''(x)dx = \frac{(n-2)(n-1)n(n+1)(n+2)(n+3)}{3}, \quad \text{(F2)}$$

and

$$P_n^3(x) = 4(1-x^2)^{\frac{1}{2}}P_{n+1}''(x) - (n+2)(n+3)P_n'(x)(1-x^2)^{\frac{1}{2}}, \quad \text{(F3)}$$

and

$$P_n^{3'}(x) = 4P_{n+1}'''(x)(1-x^2)^{\frac{1}{2}} - \frac{4x}{(1-x^2)^{\frac{1}{2}}}P_{n+1}''(x) + (n+2)(n+3)\frac{x}{(1-x^2)^{\frac{1}{2}}} - (n+2)(n+3)P_n''(x)(1-x^2)^{\frac{1}{2}}, \quad \text{(F4)}$$

then we get

$$\int_{-1}^{1} P_{n-1}^{3'}(x)P_n^3(x)dx = -(n-3)(n-2)(n-1)n(n+1)(n+2), \tag{F5}$$

$$\int_{-1}^{1} P_{n-1}^{3'}(x)P_{n+2}^3(x)dx = -(n-3)(n-2)(n-1)n(n+1)(n+2), \tag{F6}$$

and

$$\begin{aligned}\int_{-1}^{1} P_n^{3'}(x)P_{n-1}^3(x)dx &= \int_{-1}^{1} P_{n-1}^3(x)dP_n^3(x) = P_n^3(x)P_{n-1}^3(x)|_{-1}^{1} - \int_{-1}^{1} P_n^3(x)dP_{n-1}^3(x) = -\int_{-1}^{1} P_{n-1}^{3'}(x)P_n^3(x)dx \\ &= (n-3)(n-2)(n-1)n(n+1)(n+2),\end{aligned} \tag{F7}$$

$$\int_{-1}^{1} P_{n+1}^{3'}(x)P_{n+2}^3(x)dx = -(n-1)n(n+1)(n+2)(n+3)(n+4), \tag{F8}$$

$$\int_{-1}^{1} P_{n+1}^3(x)P_{n+1}^3(x)dx = \frac{2}{2n+1}\frac{(n+3)!}{(n-3)!}. \tag{F9}$$

Therefore, we have

$$\int_{-1}^{1}(1-x^2)xP_n^{3'}(x)P_{n+1}^{3'}(x)dx = \frac{(2n^3-8n-9)(n-2)(n-1)n(n+1)(n+2)(n+3)}{(2n+1)(2n+3)}, \tag{F10}$$

$$\int_{-1}^{1}(1-x^2)xP_n^{3'}(x)P_{n+1}^{3'}(x)dx + 9\int_{-1}^{1} P_n^3(x)P_{n+1}^3(x)\frac{x}{1-x^2}dx = \frac{2(n-2)(n-1)n^2(n+1)(n+2)^2(n+3)(n+4)}{(2n+1)(2n+3)}. \tag{F11}$$

The expression of the reduced SSRF for the third-order Bessel second sound (see Fig. 5) is

$$\begin{aligned}Y = &-\frac{5T_1}{3T_0}\sum_{n=3}^{\infty}\frac{2}{(n-1)n(n+1)(n+2)(n+3)}[V_n(qa)U_{n+1}(qa) - U_n(qa)V_{n+1}(qa)]P_n^3(\cos\delta)P_{n+1}^3(\cos\delta) \\ &-\frac{3T_1}{2T_0(qa)^2}\sum_{n=3}^{\infty}\frac{2}{(n-1)(n+1)(n+3)}[V_n(qa)U_{n+1}(qa) - U_n(qa)V_{n+1}(qa)]P_n^3(\cos\delta)P_{n+1}^3(\cos\delta).\end{aligned} \tag{F12}$$

APPENDIX G: REDUCED SSRF FOR THE FOURTH-ORDER BESSEL SECOND SOUND

As before, our main goal is to evaluate the following expressions: $C1 = \int_{-1}^{1} P_n^4(x)P_{n+1}^4(x)xdx$, $C2 = \int_{-1}^{1} P_n^4(x)P_{n+1}^4(x)\frac{x}{1-x^2}dx$, and $C3 = \int_{-1}^{1} x(1-x^2)P_n^{4'}(x)P_{n+1}^{4'}(x)dx$. Noting that

$$\int_{-1}^{1} xP_n^4(x)P_{n+1}^4(x)dx = \frac{n-3}{2n+1}\frac{2}{2n+3}\frac{(n+5)!}{(n-3)!}, \tag{G1}$$

$$\int_{-1}^{1} P_n^4(x)P_{n+1}^4(x)\frac{x}{1-x^2}dx = \frac{(n-3)(n-2)(n-1)n(n+1)(n+2)(n+3)(n+4)}{4}, \tag{G2}$$

and

$$\begin{aligned}&\int_{-1}^{1}(1-x^2)xP_n^{4'}(x)P_{n+1}^{4'}(x)dx \\ &= \int_{-1}^{1}\left[\frac{(n+4)P_{n-1}^{4'}(x) + (n-3)P_{n+1}^{4'}(x)}{2n+1} - P_n^4(x)\right]\left[\frac{(n+2)(n+5)P_n^4(x) - (n+1)(n-2)P_{n+2}^4(x)}{2n+3}\right]dx,\end{aligned} \tag{G3}$$

$$\begin{aligned}P_n^{4'}(x) &= 6(1-x^2)P_{n+1}^{'''}(x) - (n+3)(n+4)P_n^{''}(x)(1-x^2) \\ &= 6[4P_{n+2}^{''}(x) - (n+3)(n+4)P_{n+1}^{'}(x)] - (n+3)(n+4)[2P_{n+1}^{'}(x) - (n+1)(n+2)P_n(x)] \\ &= 24P_{n+2}^{''}(x) - 8(n+3)(n+4)P_{n+1}^{'}(x) + (n+1)(n+2)(n+3)(n+4)P_n(x),\end{aligned} \tag{G4}$$

$$P_{n-1}^{4'}(x) = 24P_{n+1}^{'''}(x) - 8(n+2)(n+3)P_n^{''}(x) + n(n+1)(n+2)(n+3)P_{n-1}^{'}(x), \tag{G5}$$

$$\int_{-1}^{1} P_{n-1}^{4'}(x)P_n^4(x)dx = -(n-4)(n-3)(n-2)(n-1)n(n+1)(n+2)(n+3), \tag{G6}$$

$$\int_{-1}^{1} P_{n-1}^{4'}(x)P_{n+2}^{4}(x)dx = -(n-4)(n-3)(n-2)(n-1)n(n+1)(n+2)(n+3), \tag{G7}$$

$$\int_{-1}^{1} P_{n}^{4'}(x)P_{n-1}^{4}(x)dx = \int_{-1}^{1} P_{n-1}^{4}(x)dP_{n}^{4}(x) = P_{n}^{4}(x)P_{n-1}^{4}(x)|_{-1}^{1} - \int_{-1}^{1} P_{n}^{4}(x)dP_{n-1}^{4}(x) = -\int_{-1}^{1} P_{n-1}^{4'}(x)P_{n}^{4}(x)dx$$
$$= (n-4)(n-3)(n-2)(n-1)n(n+1)(n+2)(n+3), \tag{G8}$$

$$\int_{-1}^{1} P_{n}^{4}(x)P_{n+1}^{4'}(x)dx = (n-3)(n-2)(n-1)n(n+1)(n+2)(n+3)(n+4), \tag{G9}$$

$$\int_{-1}^{1} P_{n}^{4^2}(x)dx = \frac{2}{2n+1}(n-3)(n-2)(n-1)n(n+1)(n+2)(n+3)(n+4), \tag{G10}$$

$$\int_{-1}^{1} P_{n+1}^{4'}(x)P_{n+2}^{4}(x)dx = -(n-2)(n-1)n(n+1)(n+2)(n+3)(n+4)(n+5), \tag{G11}$$

then we have

$$\int_{-1}^{1} (1-x^2)xP_{n}^{4'}(x)P_{n+1}^{4'}(x)dx = \frac{(n-3)(n-2)(n-1)n(n+1)(n+2)(n+3)(n+4)[2n^3-2n^2-12n-12]}{(2n+1)(2n+3)}. \tag{G12}$$

Thus we can know

$$\int_{-1}^{1} (1-x^2)xP_{n}^{4'}(x)P_{n+1}^{4'}(x)dx + 16\int_{-1}^{1} P_{n}^{4}(x)P_{n+1}^{4}(x)\frac{x}{1-x^2}dx$$
$$= \frac{(n-3)(n-2)(n-1)n(n+1)(n+2)(n+3)(n+4)[2n^3+14n^2+20n]}{(2n+1)(2n+3)}. \tag{G13}$$

And the result of the reduced SSRF (see Fig. 6) is

$$Y = -\frac{5T_1}{3T_0}\sum_{n=4}^{\infty}\frac{2}{(n-2)(n-1)n(n+1)(n+2)(n+3)(n+4)}[V_n(qa)U_{n+1}(qa) - U_n(qa)V_{n+1}(qa)]P_n^4(\cos\delta)P_{n+1}^4(\cos\delta)$$
$$-\frac{3T_1}{2T_0(qa)^2}\sum_{n=4}^{\infty}\frac{2}{(n-2)(n-1)(n+1)(n+3)(n+4)}[V_n(qa)U_{n+1}(qa) - U_n(qa)V_{n+1}(qa)]P_n^4(\cos\delta)P_{n+1}^4(\cos\delta). \tag{G14}$$

[1] Y. Li, W. Li, T. Han, X. Zheng, J. Li, B. Li, S. Fan, and C.-W. Qiu, Transforming heat transfer with thermal metamaterials and devices, Nat. Rev. Mater. **6**, 488 (2021).

[2] Z. Zhang, L. Xu, T. Qu, M. Lei, Z.-K. Lin, X. Ouyang, J.-H. Jiang, and J. Huang, Diffusion metamaterials, Nat. Rev. Phys. **5**, 218 (2023).

[3] P. Jin, J. Liu, L. Xu, J. Wang, X. Ouyang, J.-H. Jiang, and J. Huang, Tunable liquid–solid hybrid thermal metamaterials with a topology transition, Proc. Natl. Acad. Sci. (USA) **120**, e2217068120 (2023).

[4] C. Kittel and P. McEuen, *Introduction to Solid State Physics* (Wiley, New York, 2018).

[5] J. Callaway, Model for lattice thermal conductivity at low temperatures, Phys. Rev. **113**, 1046 (1959).

[6] F. Gaeta, Radiation pressure theory of thermal diffusion in liquids, Phys. Rev. **182**, 289 (1969).

[7] F. S. Gaeta, E. Ascolese, and B. Tomicki, Radiation forces associated with heat propagation in nonisothermal systems, Phys. Rev. A **44**, 5003 (1991).

[8] C. Albanese, P. Dell'Aversana, and F. S. Gaeta, Experimental Detection of Forces Produced by the Flow of Heat, Phys. Rev. Lett. **79**, 4151 (1997).

[9] M. Braibanti, D. Vigolo, and R. Piazza, Does Thermophoretic Mobility Depend on Particle Size?, Phys. Rev. Lett. **100**, 108303 (2008).

[10] A. Würger, Hydrodynamic Boundary Effects on Thermophoresis of Confined Colloids, Phys. Rev. Lett. **116**, 138302 (2016).

[11] R. Guyer and J. Krumhansl, Thermal conductivity, second sound, and phonon hydrodynamic phenomena in nonmetallic crystals, Phys. Rev. **148**, 778 (1966).

[12] E. Prohofsky and J. Krumhansl, Second-sound propagation in dielectric solids, Phys. Rev. **133**, A1403 (1964).

[13] L. Xu, G. Xu, J. Huang, and C.-W. Qiu, Diffusive Fizeau Drag in Spatiotemporal Thermal Metamaterials, Phys. Rev. Lett. **128**, 145901 (2022).

[14] L. Xu, G. Xu, J. Li, Y. Li, J. Huang, and C.-W. Qiu, Thermal Willis Coupling in Spatiotemporal Diffusive Metamaterials, Phys. Rev. Lett. **129**, 155901 (2022).

[15] B. D. Coleman and D. C. Newman, Implications of a nonlinearity in the theory of second sound in solids, Phys. Rev. B **37**, 1492 (1988).

[16] G. M. Tarkenton and M. S. Cramer, Nonlinear second sound in solids, Phys. Rev. B **49**, 11794 (1994).

[17] G. M. Tarkenton and M. S. Cramer, Arrival times for dissipative, nonlinear second-sound waves in solids, Phys. Rev. B **52**, 24 (1995).
[18] H. E. Jackson, C. T. Walker, and T. F. McNelly, Second Sound in NaF, Phys. Rev. Lett. **25**, 26 (1970).
[19] V. Narayanamurti and R. Dynes, Observation of Second Sound in Bismuth, Phys. Rev. Lett. **28**, 1461 (1972).
[20] D. Osborne, Second sound in liquid helium II, Proc. Phys. Soc. A **64**, 114 (1951).
[21] A. Beardo, M. López-Suárez, L. A. Pérez, L. Sendra, M. I. Alonso, C. Melis, J. Bafaluy, J. Camacho, L. Colombo, R. Rurali *et al.*, Observation of second sound in a rapidly varying temperature field in Ge, Sci. Adv. **7**, eabg4677 (2021).
[22] S. Huberman, R. A. Duncan, K. Chen, B. Song, V. Chiloyan, Z. Ding, A. A. Maznev, G. Chen, and K. A. Nelson, Observation of second sound in graphite at temperatures above 100 K, Science **364**, 375 (2019).
[23] Z. Ding, K. Chen, B. Song, J. Shin, A. A. Maznev, K. A. Nelson, and G. Chen, Observation of second sound in graphite over 200 K, Nat. Commun. **13**, 1 (2022).
[24] X. Li, X. Luo, S. Wang, K. Xie, X.-P. Liu, H. Hu, Y.-A. Chen, X.-C. Yao, and J.-W. Pan, Second sound attenuation near quantum criticality, Science **375**, 528 (2022).
[25] P. C. Kwok, Dispersion and damping of second sound in non-isotropic solids, Phys. Phys. Fiz. **3**, 221 (1967).
[26] H. Beck, P. Meier, and A. Thellung, Phonon hydrodynamics in solids, Phys. Status Solidi A **24**, 11 (1974).
[27] J. Ward and J. Wilks, The velocity of second sound in liquid helium near the absolute zero, London Edinburgh Dublin Philos. Mag. J. Sci. **42**, 314 (1951).
[28] Dingleand R. B, Derivation of the velocity of second sound from maxwell's equation of transfer, Proc. Phys. Soc. A **65**, 374 (1952).
[29] J. Sussmannand A. Thellung, Thermal conductivity of perfect dielectric crystals in the absence of umklapp processes, Proc. Phys. Soc. **81**, 1122 (1963).
[30] O. A. Sapozhnikovand M. R. Bailey, Radiation force of an arbitrary acoustic beam on an elastic sphere in a fluid, J. Acoust. Soc. Am. **133**, 661 (2013).
[31] Z. Gongand M. Baudoin, Acoustic radiation torque on a particle in a fluid: An angular spectrum based compact expression, J. Acoust. Soc. Am. **148**, 3131 (2020).
[32] G. T. Silva, An expression for the radiation force exerted by an acoustic beam with arbitrary wavefront (L), J. Acoust. Soc. Am. **130**, 3541 (2011).
[33] D. Baresch, J.-L. Thomas, and R. Marchiano, Three-dimensional acoustic radiation force on an arbitrarily located elastic sphere, J. Acoust. Soc. Am. **133**, 25 (2013).
[34] G. Silva, T. Lobo, and F. Mitri, Radiation torque produced by an arbitrary acoustic wave, Europhys. Lett. **97**, 54003 (2012).
[35] Z. Gong, P. L. Marston, and W. Li, Reversals of Acoustic Radiation Torque in Bessel Beams Using Theoretical and Numerical Implementations in Three Dimensions, Phys. Rev. Appl. **11**, 064022 (2019).
[36] Z. Gongand M. Baudoin, Equivalence between angular spectrum-based and multipole expansion-based formulas of the acoustic radiation force and torque, J. Acoust. Soc. Am. **149**, 3469 (2021).
[37] M. Chester, Second sound in solids, Phys. Rev. **131**, 2013 (1963).
[38] P. L. Marston, Axial radiation force of a bessel beam on a sphere and direction reversal of the force, J. Acoust. Soc. Am. **120**, 3518 (2006).
[39] J. Arltand K. Dholakia, Generation of high-order bessel beams by use of an axicon, Opt. Commun. **177**, 297 (2000).
[40] N. Jiménez, R. Picó, V. Sánchez-Morcillo, V. Romero-García, L. M. García-Raffi, and K. Staliunas, Formation of high-order acoustic bessel beams by spiral diffraction gratings, Phys. Rev. E **94**, 053004 (2016).
[41] L. Zhangand P. L. Marston, Geometrical interpretation of negative radiation forces of acoustical Bessel beams on spheres, Phys. Rev. E **84**, 035601(R) (2011).
[42] P. L. Marston, Negative axial radiation forces on solid spheres and shells in a bessel beam, J. Acoust. Soc. Am. **122**, 3162 (2007).
[43] F. G. Mitri, Langevin acoustic radiation force of a high-order bessel beam on a rigid sphere, IEEE Trans. Ultrason. Ferroelectr. Freq. Control **56**, 1059 (2009).
[44] Marstonand L. Philip, Radiation force of a helicoidal bessel beam on a sphere, J. Acoust. Soc. Am. **125**, 3539 (2009).
[45] M. Gong, Y. Qiao, Z. Fei, Y. Li, J. Liu, Y. Mao, A. He, and X. Liu, Non-diffractive acoustic beams produce negative radiation force in certain regions, AIP Adv. **11**, 065029 (2021).
[46] M. Baudoinand J.-L. Thomas, Acoustic tweezers for particle and fluid micromanipulation, Annu. Rev. Fluid Mech. **52**, 205 (2020).
[47] J. Chen, J. Ng, Z. Lin, and C. T. Chan, Optical pulling force, Nat. Photon. **5**, 531 (2011).
[48] D. Pan, H. Xu, and F. de Abajo, Emergence of material momentum in optical media, arXiv:1907.04947 (2019).
[49] H. Li, Y. Cao, B. Shi, T. Zhu, Y. Geng, R. Feng, L. Wang, F. Sun, Y. Shi, M. A. Miri, N.-V. Manuel, C.-W. Qiu, and W. Ding, Momentum-Topology-Induced Optical Pulling Force, Phys. Rev. Lett. **124**, 143901 (2020).
[50] X.-D. Fanand L. Zhang, Phase shift approach for engineering desired radiation force: Acoustic pulling force example, J. Acoust. Soc. Am. **150**, 102 (2021).
[51] J. T. Karlsen, P. Augustsson, and H. Bruus, Acoustic Force Density Acting on Inhomogeneous Fluids in Acoustic Fields, Phys. Rev. Lett. **117**, 114504 (2016).
[52] P. L. Palla, G. Patera, F. Cleri, and S. Giordano, A stochastic force model for the ballistic-diffusive transition of heat conduction, Phys. Scr. **95**, 075703 (2020).
[53] S. Lepri, R. Livi, and A. Politi, Thermal conduction in classical low-dimensional lattices, Phys. Rep. **377**, 1 (2003).
[54] A. Dhar, Heat transport in low-dimensional systems, Adv. Phys. **57**, 457 (2008).
[55] M. Gerl, Calculation of the force acting on an impurity in a metal submitted to an electric field or a temperature gradient, Z. Naturforsch. A **26**, 1 (1971).
[56] R. S. Sorbello, Phonon-radiation force in defect crystal lattices, Phys. Rev. B **6**, 4757 (1972).